Article

Not peer-reviewed version

Sulfides, Sulfosalts and Sulfates in the Epithermal Au-Ag-Te Emmy Deposit (Khabarovsk Territory), Far East, Russia: Implications for the Mineralization Process

Tamara Yu. Yakich *, Panagiotis Voudouris, Darya V. Levochskaia, Alexey K. Mazurov, Michail V. Shaldybin, Yuriy M. Lopushnyak, Alexey S. Ruban, Alexey E. Erofeev, Mikhail S. Minakov, Prokopiy N. Maximov, Ekaterina A. Sinkina, Ksenia V. Bestemianova, Maxim A. Rudmin

Posted Date: 16 August 2024

doi: 10.20944/preprints202408.1245.v1

Keywords: epithermal Au-Ag-Te emmy deposit; far east; pyrite; oscillatory zoning; sulfosalts; Aluminum-Phosphate-Sulfate (APS) minerals

Article

Sulfides, Sulfosalts and Sulfates in the Epithermal Au-Ag-Te Emmy Deposit (Khabarovsk Territory), Far East, Russia: Implications for the Mineralization Process

Tamara Yu. Yakich [1,*], Panagiotis Voudouris [2], Darya V. Levochskaia [3], Alexey K. Mazurov [1], Mikhail V. Shaldybin [1,4], Yuriy M. Lopushnyak [5], Alexey S. Ruban [1], Alexei E. Erofeev [3], Mikhail S. Minakov [1], Prokopiy N. Maximov [1], Ekaterina A. Sinkina [1], Ksenia V. Bestemianova [6] and Maxim A. Rudmin [1]

[1] School of Earth Sciences & Engineering, Division for Geology, Tomsk Polytechnic University, 634050 Tomsk, Russia, cherkasovatu@tpu.ru
[2] Faculty of Geology and Geoenvironment, National and Kapodistrian University of Athens, GR-15784, Zografou, Athens, Greece, voudouris@geol.uoa.gr
[3] Khabarovsk Branch of JSC "Polymetal UK", 680000 Khabarovsk, Russia, levochskayaDV@polymetal.ru
[4] JSC "TomskNIPIneft", 634027 Tomsk, Russia, shaldybinmv@yandex.ru
[5] LLC "NPP Qualitet"140000, Moscow, Russia, lum83@mail.ru
[6] Laboratory of geochronology and geodynamics, department of Geology and Geography, Tomsk State University, 634050 Tomsk, Russia; KsenijaVT@mail.ru
* Correspondence: cherkasovatu@tpu.ru

Abstract: This study considers the features of the chemical composition, internal structure, and oscillatory zoning of sulfides, sulfosalts and sulfates in the epithermal high-intermediate sulfidation type Au-Ag-Te Emmy deposit (Khabarovsk Territory), Russia. In this deposit the most widespread sulfide is pyrite occurring in two generations: pre-ore pure pyrite (I) with cubic crystal habit and dimensions from 20 μm to 0.5 mm from the early barren pre-ore hydrothermal stage, and pyrite (II) of the ore stage, which is represented by (a) colloform aggregates (IIa) formed as a result of rapid precipitation from the solution, and (b) crystalline pyrite (IIb), which is precipitated due to continuous decrease in temperature. Both pyrite (II) morphological varieties contain copper (0.06-6.03 wt.%). The crystalline variety of pyrite is associated with goldfieldite, hemusite and kawazulite which were deposited during the early mineralizing event in the deposit. At Emmy deposit, sulfosalts are mainly represented by goldfieldite probably corresponding to a high-sulfidation (HS) mineral association, and by tennantite-tetrahedrite group minerals. The latter are associated with tellurides and native tellurium corresponding to an intermediate-sulfidation (IS) type ore assemblage and suggesting increasing influx of Te, Sb and As in the system. Goldfieldite is replaced by native tellurium and tellurides along its growth zones, and is characterized by oscillatory zoning. The observed replacement of goldfieldite by the tellurides of mercury, nickel, lead and copper, indicates a new influx of volatiles including native gold, native tellurium, gold-silver tellurides into the open mineral-forming system. At deeper levels of the Emmy deposit, an advanced argillic alteration assemblage includes aluminium-phosphate-sulfate (APS) minerals, represented by members of the svanbergite-woodhouseite series. Element mapping of the studied APS mineral grains, indicated three distinct areas recording the evolution of the hydrothermal system at Emmy: an oscillatory zoned margin enriched in sulfur, lead and barium, corresponding to the late influx of IS state fluids related to gold and tellurides, an intermediate part which is leached and correspond to the HS mineralization stage, while the central part of the grains is enriched in cerium, calcium and strontium, resulted as a replacement of magmatic apatite in the pre-ore alteration stage. The leached zone between core and rim of the APS grains is related to a change in crystallization conditions, possibly due to boiling or mixing processes of the fluids. Barite found in the upper level of the advanced argillic alteration assemblage, is also characterized by oscillatory zoning associated

 doi:10.20944/preprints202408.1245.v1

with the enrichment of individual zones in lead. Associated with this barite are micron gold particles confined to lead-enriched zones, filling the pore space in the barite. This study demonstrates that nature of oscillatory zoning in sulfosalts and sulfates at the Emmy deposit is a result of external process. Such process is of fundamental importance from both a genetic and exploration point of view.

Keywords: epithermal Au-Ag-Te emmy deposit; far east; pyrite; oscillatory zoning; sulfosalts; Aluminum-Phosphate-Sulfate (APS) minerals

1. Introduction

Epithermal gold deposits are low-temperature deposits (< than 300°C), usually located at depths of up to 1000 km [1], often accompanied by advanced argillic and silicic alteration [1–4]. In Russia, such deposits are widespread within the Far East, including both recent [5] and ancient (Cretaceous age) [6] Pacific rim epithermal deposits. This type of ore deposit, has recently attracted increased significance in Russia, although previously not considered as a gold source, due to the complexity of enrichment and the small size of gold particles. This is mainly because, in addition to gold and silver, these deposits contain a significant amount of associated useful metals/metalloids such as Te, As, Bi, Se, Sb (TABSS), which are trace elements in other setting. Moreover, the established relationship between the critical TABSS-elements and precious metals can be used as sensitive indicators of the conditions for the formation of epithermal deposits and mineralization processes. TABSS-elements can form their own mineral phases, as well as they can incorporate as trace elements in major sulfides and in sulfosalts, thereby demonstrating fluid fluctuations during ore deposition and the various stages of ore concentration.

Minerals which host trace TABSS-elements can act as markers of changes in physicochemical conditions (redox potential, pH, fluid parameters as for example, sulfidation-oxidation reactions at redox fronts). Of particular interest in this sense are sulfides, sulfosalts and tellurides, which accompany precious metals in ore deposits [7–11]. For example, gold and silver tellurides themselves can constitute a significant proportion of the total gold budget in a deposit [12,13]. Worldwide hundreds of such deposits are known with some examples given below: Cripple Creek and Golden Sunlight gold-silver-telluride deposits in the U.S.A. (Montana) [14], Emperor (Fiji) [15], Dongping gold deposit (Hebei Province, China) [16], Acupan and Baguio gold-silver-telluride districts (Philippines) [17], Sacarimb deposit (Romania) [18], Kochbulak gold-telluride deposit (Uzbekistan) [19,20], Perama Hill Au-Ag-Te-Se deposit (Greece) [21], Maletoyvayam deposit (Koryak Highland, Russia) [22,23] and Emmy gold-silver-telluride deposit (Khabarovsk Territory, Russia) [24,this study]. The formation of such deposits has been associated with deposition from fluids rich in TABSS-elements formed under certain regional conditions, for example, due to the subduction of tellurium-rich sediments of the ocean floor, as can be observed within the Pacific Rim.

Bulk ore data of precious metal bearing epithermal deposits provide little genetic information about the sources, transport modes, fluctuations of the ore-bearing solution, and the process of mineralization. Features of the mineral-chemical composition, crystal habit and internal structure of accompanying minerals, can be more informative in this respect. So, for example, oscillatory zoning – periodically repeating maxima and minima of the values of any component of the crystal, as a process of organization of matter in the process of hydrothermal mineral formation, is often encountered [25–28]. The factors that control the oscillatory zoning of minerals can be both internal (i.e. self-organization mechanisms), due to the ability of a crystal to absorb one or another component to varying degrees – such zoning is individual for each crystal, and external (general), as a rule, the nature of zoning is preserved in different grains, the amount of bands in adjacent crystals is the same [26–28]. The last type of zoning is the most interesting and informative, as it may indicate any periodic changes in the mineral-forming environment. According to Holten et al. [27] oscillatory mineral zonation is usually associated with crystal growth in an open system and is characterized by non-

 doi:10.20944/preprints202408.1245.v1

equilibrium states. The resulting zonation patterns will be the result of coupling between the generally nonlinear crystal growth dynamics and the boundary conditions imposed by externally controlled fluctuation.

This study expands on previous work from Yakich et al. [24] on the Svetloye epithermal district, Okhotsk-Chukotka volcanic belt, and presents new data on sulfosalt, sulfide, telluride and sulfate mineralogy of the Emmy deposit in this field. Emphasis is given in oscillatory zoned minerals in the deposit, namely goldfieldite (a member of the tetrahedrite group [29]), as well as on aluminum-phosphate-sulfate (APS) minerals (members of the alunite supergroup minerals [30–34]), and barite, which form part of the advanced argillic alteration assemblage and described here for the first time from the deposit. We use oscillatory zoning as a tool for decoding the genetic information contained in sulfosalts and sulfates crystals, aiming in reconstructing conditions of deposit formation.

2. Geological Background

2.1. Geology of the Emmy Deposit

The gold-silver telluride Emmy deposit is part of the Svetloye epithermal gold ore district, which, in turn, is confined to the Ul'insky trough, composed of Cretaceous volcanic formations of the Okhotsk-Chukotka volcanic belt [35]. The Svetloye ore district contains several deposits: Emmy, Lyudmila, Elena, Tamara and Larisa (Figure 1). The Emmy deposit is confined to the northwestern volcanic edifice of Coniacian-Santonian age (K_2), and differs from all others deposits of the Svetloye ore district by the presence of abundant telluride mineralization not found in the other deposits confined to the southeastern volcanic center (Elena, Tamara, Lyudmila, and Larisa deposits). The latter are hosted within the dacite-rhyolite-leucogranite formation of the Urak suite (Campanian-Maastrichtian time age (K_2). The Khetanian Suite hosting the Emmy deposit is represented by andesites, basaltic andesites, their agglomerate lavas, and more rarely tuffs (Figure 1). The most widely developed pyroxene andesites are dark gray, almost black in color.

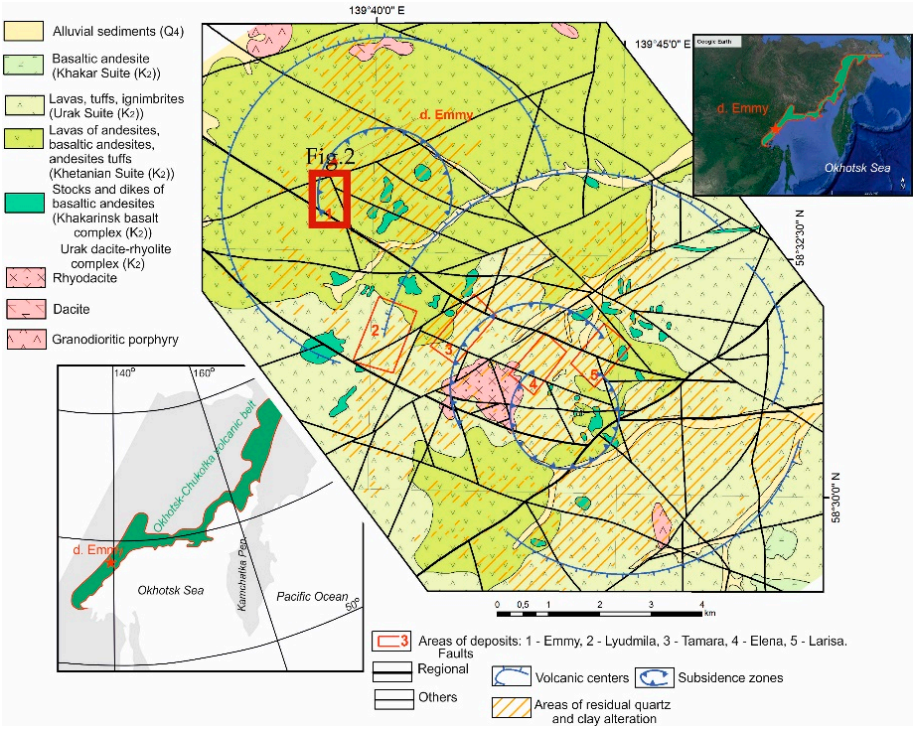

Figure 1. Schematic geological map of the epithermal Au-Ag-Te Emmy deposit within the Svetloye ore district on the basis of data from B.A. Novoselov, PD Rus LLC and Ananyev et al. [36].

The deposit occurs in the form of linear keel-shaped ore bodies with mushroom-shaped swellings. The dimensions of the ore bodies are significantly variable. The length can reach 500-700m,

 doi:10.20944/preprints202408.1245.v1

with a width of 100-250m, and a thickness of 12-60m extending downward to paleo-vents up to 110 m deep. The dip of the ore zones is gentle, near the paleo-vents it is steep with an uneven or very uneven nature of the distribution of the metallic mineralization. The Emmy deposit has Au reserves of 14.6t with an average grade of 2.65 g/t Au. Two types of gold mineralization are distinguished: Au-Ag-telluride and Au-Ag [24]. It is classified as HS-IS type [22]. However, it lack of high-sulfidation-state sulfides/sulfosalts such as hypogene covellite, enargite, famatinite, luzonite probably due to their erosion at shallower paleodepth, and/or to their supergene oxidation below the present day surface [24].

2.2. Alteration Zones

Based on the results of mineralogical and petrographic studies of 120 hand specimens and its thin sections and using interpretation of ASTER data [37], a schematic map and cross-section of hydrothermal alteration mineral zones for the Emmy deposit was developed (Figure 2a-b). It was established that within the Emmy deposit, the wall-rock alteration of the host rocks is mainly represented by residual quartz and brecciated residual quartz (Figure 2c-d), to a lesser extent alunite- and dickite-bearing advanced argillic alteration (Figure 2e-f) as well as quartz-white mica altered rocks (Figure 2g). In the latter alteration zone, the primary host andesitic rocks and their tuffs display various degrees of alteration with the relict outlines of porphyritic phenocrysts replaced by sericite, muscovite or illite (Figure 2h) [6].

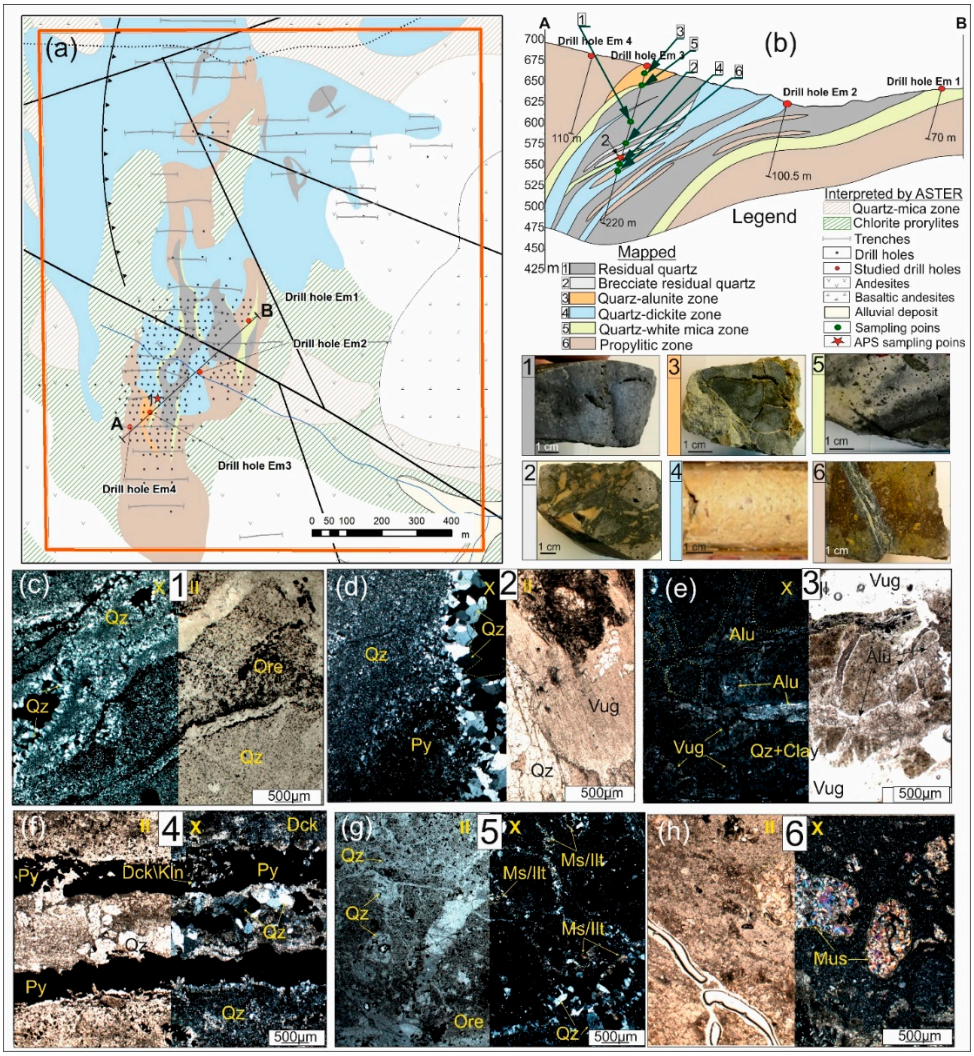

Figure 2. (**a**) Schematic map of hydrothermal alteration zones and (**b**) geological cross section (AB) of the Emmy deposit, according to the author's data (hand specimens (1-6) and thin sections (**c-h**)), and

 doi:10.20944/preprints202408.1245.v1

data obtained from ASTER images [37]. Photographs of hand specimens and transmitted-light microphotographs of thin sections in plane (II)- and cross (X)-polarized light of the main varieties of altered rocks: (**c**) Residual vuggy quartz zone with comb quartz (Qz) filling vugs, and dissemination of ore minerals (Ore); (**d**) Brecciated residual quartz zone with rock fragments composed of groundmass of allotriomorphic, fine-grained microgranular quartz and unevenly distributed ore dissemination (Ore). Zoned crystals of euhedral quartz (Qz) overgrow cavities (Vug); (**e**) Quartz-alunite zone with alunite (Alu) in veinlets and also filling voids (Vug) of the quartz (Qz); (**f**) Quartz-dickite zone composed of fine-grained quartz (Qz) and dickite/kaolinite (Dck/Kln) with Pyrite (Py) of first ore phase associated with comb quartz; (**g**) Quartz (Qz)-white mica (Mus/Ilt) altered rock with disseminated pyrite with other metallic minerals (Ore) and muscovite/illite-quartz veinlets; (**h**) Muscovite-altered andesite with relic plagioclase phenocrysts replaced by white mica (Mus) into quartz altered groundmass.

Mineralogy and Petrographic Description of Altered Rocks

Residual quartz zone: The groundmass of the rocks is composed of allotriomorphic, granular (0.01-0.02 mm in size) quartz, among which larger quartz grains (up to 1 mm) are observed. The rock is penetrated by many differently oriented mutually intersecting cracks (Figure 2c; hand specimen No 1). The cracks are completely filled with euhedral quartz, forming a system of intersecting veinlets. Relatively large cracks (up to 4 mm) are locally characterized by open spaces and druses.

Three generations of quartz have been distinguished: generation (i) is allotriomorphic, micro- and, less often, fine-grained quartz, which makes up the bulk of the rock; generation (ii) – (a) fine-grained quartz, growing along cracks and (b) comb well-crystallized quartz - filling cracks and vugs, and also forming clusters up to 2 mm in diameter in the groundmass of the rock, and generation (iii) accompanied by tellurides. The silicified rock is characterized by a high content of opaque minerals (more than 5 vol. %), mainly represented by pyrite. Opaque minerals form linear (Figure 2c,f) and cluster-like assemblages (Figure 2d), and can also be present as sporadic grains regularly dispersed in the groundmass.

The residual vuggy quartz zone is the most abundant rock type compared to other structural and textural rock varieties occurring within the Emmy deposit. The size of the vugs varies from 0.05 to 2 mm (average 0.2 mm), with vugs covering up to 50% of the total volume of the thin section area. The vugs are characterized by overgrowth textures, characterized by the development of euhedral quartz along the walls of the vug's open spaces (Figure 2c).

Brecciated residual quartz zone is represented by quartz developing in the matrix cementing clasts of silicified volcanic rocks. Comb quartz is sometimes observed, which overgrows large cavities (Figure 2d). The groundmass of the silicified rock fragments is composed of allotriomorphic granular quartz (0.01–0.03 mm) with disseminated pyrite. Quartz in the sililcified fragments is fractured and crosscut by quartz-pyrite veinlets. Pyrite dissemination has a streaky mass character. Pyrite is brecciated and associated with prismatic rutile crystals.

Quartz-alunite zone is characterized by a porphyroblastic texture (Figure 2e). The rock is composed of a dark brown microcrystalline quartz–clay aggregate fractured by cracks up to 1 mm wide (Figure 2e). The cracks are filled with coarse-grained alunite represented by long-prismatic crystals up to 0.01 mm in size. In addition to filling cracks, alunite forms monomineralic clustered aggregates with a diameter of up to 1 mm. In these clusters, alunite has needle-shaped crystals up to 0.2 mm in size. APS are not found in this zone, but barite may occur.

Quartz-dickite zone is composed of fine-grained quartz (0.01-0.05 mm) of allotriomorphic texture associated with fine dickite/kaolinite flakes, among which larger grains of quartz (up to 0.5 mm) are often distinguished. The content of dickite/kaolinite is about 15 vol.% of the section area. In the groundmass, there are zones with crystals of euhedral quartz, having a zonal structure, ranging in size from 0.5-1 mm, with cavities between crystals up to 2 mm. Quartz aggregates have a mosaic-block structure. This zone is associated with ore mineralization represented mainly by pyrite deposited from the first ore phase, which can form elongated zones (Figure 2f). In this zone at a depth of 130-150 m from top drill hole Em 3 (Figure 2b, APS sampling point is marked with an asterisk) APS minerals are present.

 doi:10.20944/preprints202408.1245.v1

Quartz-white mica zone found as interlayers between residual vuggy quartz and quartz-dickite zones. This zone is observed both in shallow levels (Figure 2b,g) and at a depth of about 100-120 m within the drill hole Em 3. In the intergranular space, the development of clay minerals such as kaolinite/dickite and pyrophyllite (at depth) are observed. The groundmass of the rock is composed of allotriomorphic, granular (0.01-0.02 mm) quartz. Fan-shaped aggregates of muscovite/illite crystals stand out among the quartz–clay aggregate (Figure 2g). The groundmass contains numerous vugs ~ 0.5 mm in diameter. Comb, euhedral quartz (overgrowth textures) develops along the walls of the vugs, up to the complete filling of the vugs. The rock is crosscut by numerous cracks up to 2 mm wide, with an average thickness of 0.5 mm. The cracks are filled with quartz (grain sizes up to 1 mm) and muscovite/illite (up to 0.5 mm) and metallic minerals. Ore mineralization occurs in veinlets and in the form of disseminations uniformly dispersed in the groundmass (Figure 2g). The grain sizes of metallic minerals do not exceed 0.02 mm.

This zone contains APS minerals. They occur in a drill hole not shown in the cross-section at a depth of 117.8 m from the drill head (Figure 2b). Their location is marked with an asterisk No1 only on the map (Figure 2a).

3. Samples and Methods

One hundred twenty samples of altered rocks and ores were collected from four drill holes and surface outcrops in the Emmy deposit. Fifty polished blocks and one hundred twenty thin sections of samples from mineralized veins and alteration zones were studied by electronic and optical microscopy. Suitable thin sections and polished sections were selected for the study of major and trace element analyses and mineral detection. Back scattered electron (BSE) images were taken using a TescanVega 3 SBU scanning electron microscope equipped with an energy dispersive spectrometer (EDS) of Oxford Instruments (Tomsk city, Tomsk Polytechnic University, Russia) with an Aztec-based system of microanalysis and TescanVega 2 LMU scanning electron microscope combined with Oxford Instruments INCA Energy 350 energy dispersive spectrometer and cathodoluminescence (CL) detector (Tomsk city, Tomsk State University, Russia). The operating conditions were in the high-vacuum mode (<9 × 10^{-3} Pa) at an accelerating voltage of 20 kV with a high resolution and a distance of 15 mm. Measurement parameters of accelerating voltage 10-20 kV, beam current 1.2-3.5 nA, beam size 180-500 nm. The EDS detector was calibrated using Co standard K-series 10.0063 eV, peak area 350050. Samples containing APS were analyzed using powder X-ray diffraction of bulk samples. XRD-patterns were recorded using Rigaku Ultima IV X-ray diffractometer, with a Cu anode, the X-ray tube voltage of 40 kV, the current of 30 mA, and a power of 1.2 kW. Whole rock samples were scanned from 5 to 60◦ 2θ at a scanning speed 1◦ per minute with a step of 0.02◦. In addition to the bulk samples, clay fractions were also separated by sedimentation following disaggregation and dispersion. In order to fully characterize the clay minerals, the clay fractions were scanned in the air dried state, then after saturation with glycol overnight and after heat treatment at 550◦C for 1 h. Comprehensive identification of the clay minerals was made following procedures given by Moore and Reynolds [38]. Quantitative mineralogical analyses of the whole rock data were performed by a Rietveld analysis [39] using PDXL and Siroquant software [40].

4. Results

4.1. Sulfides

The most common sulfide, especially in gold deposits, is traditionally considered to be pyrite [41–45]. The Emmy deposit is no exception, in which the main sulfide is pyrite, which occurs in several generations and crystal forms:

Pre-ore pyrite (I) with cubic habit, is fine-grained with an average crystal size of 20-50 μm to 500 μm. It is almost pure pyrite and corresponds to the early barren stage (Figure 3a). Pyrite (I) hosts inclusions of galena, sphalerite, tetrahedrite group minerals (TGM), carbonates and quartz, filling voids in the process of further mineral formation.

 doi:10.20944/preprints202408.1245.v1

Pyrite (II) from the ore stage is represented by two morphological varieties – colloform (IIa) (Figure 3b), most likely earlier, which is overgrown by crystalline (idiomorphic) pyrite (IIb) (Figure 3c). Both morphological varieties contain Cu (0.06–6.03 wt %). Pyrite of this stage occurs in association with goldfieldite (Figure 3b), hemusite (Figure 3c-d), kawazulite (Figure 3e), and replaced by tetrahedrite-tennantite, chalcopyrite (Figure 3f-i), gold-, silver- and other tellurides (Figure 3g-m), suggesting influx of later fluids enriched in Cu, Ni, Pb, Hg, Au, Ag and tellurium. Crystalline pyrite (IIb) has euhedral crystal habit that deviates from cubic depending on the depth of formation. For example, at deeper levels, pyrite (IIb) is represented by pentagondodecahedrons (i.e. pyritohedron) (Figure 3j), whereas, towards the surface, it acquires a predominantly prismatic shape. Pyrite IIb also display chemical heterogeneity in respect to its depth of formation; it is practically pure at deepest levels, it contains copper at intermediate depths (~ 38-46 m), where it is associated with colloform pyrite (IIa), and it is enriched with arsenic close to the surface.

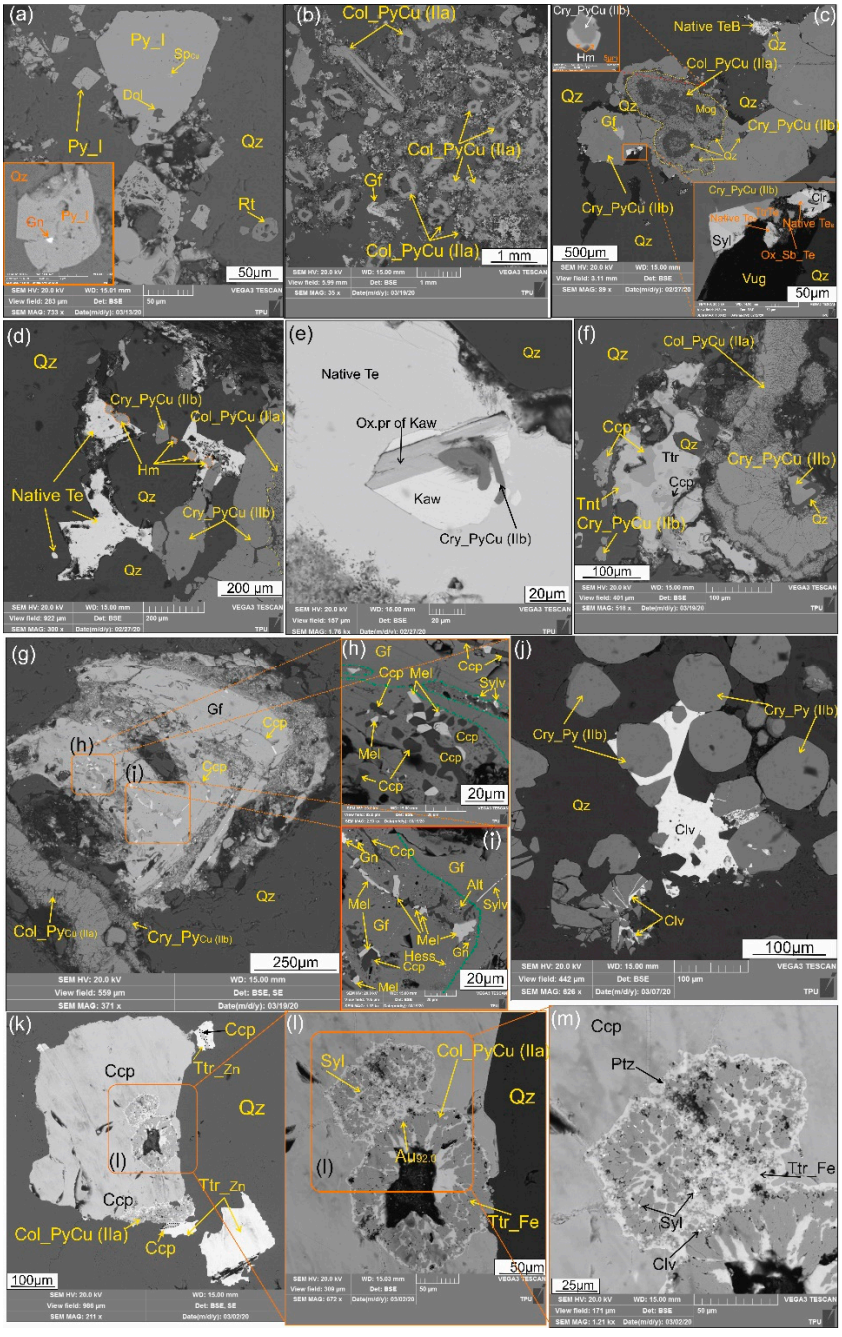

Figure 3. Microphotographs (SEM-BSE images) demonstrating sulfide, sulfosalt and telluride assemblages at Emmy deposit: (**a**) Pyrite crystals (Py_I) with cubic habit in association with rutile (Rt)

 doi:10.20944/preprints202408.1245.v1

and leached pyrite crystals (Py_I) host epigenetic inclusions of sphalerite (Sp_{Cu}), galena (Gn) and dolomite (Dol). Quartz (Qz) is the gangue; (**b**) Numerous clustered aggregates of colloform pyrite IIa containing Cu (Col_PyCu (IIa) in association with goldfieldite (Gf); (**c**) Colloform aggregate of pyrite IIa(Col_PyCu (IIa)), overgrown by crystalline pyrite II (Cry_PyCu (IIb)) in paragenetic association with hemusite (Hm) and later sylvanite (Syl), native tellurium with B (Native Te_B), tetrahedrite with Te (Ttr_{Te}), coloradoite (Clr), and TGM oxidation products (Ox_Sb_Te) crystallized in vugs of euhedral quartz (Qz); (**d**) Assemblage of colloform (Col_PyCu (IIa)) and crystalline (Cry_PyCu(IIb)) pyrite with hemusite (Hm), cemented by native tellurium (Te) in vugs of euhedral quartz (Qz); (**e**) Kawazulite (Kaw) intergrown with prismatic pyrite (Cry_PyCu(IIb)) and partly replaced by oxidation products of kawazulite, all included in native tellurium (Te) and accompanied by quartz (Qz);(**f**) Two morphology varieties of Cu-bearing pyrite, represented by idiomorphic crystals (Cry_PyCu (IIb) and colloform aggregates (Col_PyCu (IIa)). Tennantite (Tnt) and tetrahedrite (Ttr) intergrown with chalcopyrite (Ccp) overgrowing pyrite II aggregates; (**g-i**) Assemblage of colloform (Col_PyCu (IIa)) and crystalline (Cry_PyCu(IIb)) pyrite with goldfieldite (**g**), and enlarged fragments (**h-i**) demonstrated replaced areas of golfieldite (Gf) by chalcopyrite (Ccp) with melonite (Mel), galena (Gn), sylvanite (Sylv), altaite (Alt), and hessite (Hess); (**j**) Calaverite (Clv) filling gaps between euhedral quartz (Qz) crystals and rims pyritohedron pyrite crystals (Cry_Py (IIb)); (**k-m**) Inclusions of colloform pyrite IIa (Col_PyCu (IIa) replaced by tetrahedrite-(Fe) (Ttr_{Fe}) in chalcopyrite, in association with tetrahedrite-(Zn) (Ttr_{Zn}). The intergranular space of colloform pyrite is filled with tetrahedrite-(Fe) (Ttr_{Fe}), sylvanite (Syl), petzite (Ptz), calaverite (Clv) and native gold ($Au_{92.0}$).

4.1. Sulfosalts

Tetrahedrite group minerals (TGM) [46] is a widespread group of sulfosalts in hydrothermal gold deposits, and can be a sensitive indicator of the composition of the initial solutions involved in the formation of deposits [47–52]. Given the ability of TGM to form solid solutions, they are a suitable petrogenetic tool for determining the environment of mineral formation [48,53–55]. The composition of TGM can directly depend on the composition of metal-bearing solutions involved in the formation of deposits. Thus, the composition of the TGM and the nature of its internal structure can be used as an indicator of the physicochemical conditions at the time of mineral formation.

A variety of sulfosalts are developed in the Emmy deposit (Figures 3 and 4): *tennantite-tetrahedrite* with a significant variation in composition corresponding to the general formula $(Cu_{1.28-12.0}Ag_{0.0-8.65}Fe_{0.0-1.44}Zn_{0-1.74})(Sb_{0.0-3.88}As_{0.0-4.0}Bi_{0.0-0.51}Te_{0.0-2.68})S_{13}$ (Table 1) (Figure 3, f,l-m); *bournonite* $Pb_{0.83-0.96}(Cu_{0.90-1.09}Fe_{0.0-0.91})(Sb_{0.64-0.98}As_{0.0-0.41})S_3$, most likely due to the replacement of earlier galena; *emplectite* in the form of single micron-sized grains in pyrite, corresponding to the formula $(Cu_{0.42-0.45}Fe_{0.40-0.46})(Bi_{0.69-0.65}Ag_{0.07-0.09})(S_{1.96}Se_{0.04})$.

Goldfieldite attracts the most author's attention in this paper due to its important role in the mineralization: goldfieldite provides physicochemical constraints on ore formation, which help understanding trace element distribution and fluid flow paths within the deposit, and can be used to aid mineral exploration [56]. Recently, two varieties of goldfieldite have been approved by IMA, namely, stibiogoldfieldite [57] and arsenogoldfieldite [58]. At Emmy deposit both *stibiogoldfieldite* and *arsenogoldfieldite* $(Cu_{9.93-12.0}Ag_{0-0.36}Fe_{0.0-1.74})(Te_{1.41-2.68}Sb_{0.0-2.54}Bi_{0.0-0.28}As_{0.0-1.28})S_{13}$ (Table 1) contain later sylvanite $(Au_{0.86-1.67}Ag_{04-2.31}Fe_{0.06-0.39}Mo_{0.2-0.77}Ta_{0.04-0.08}Te_4)$, coloradoite $(Hg_{0.77-0.94}Te)$, melonite $(Ni_{0.92-1.00}Te_2)$ replacing goldfieldites along their growth zones (Figure 3g-i). *Goldfieldite* at Emmy deposit is characterized by oscillatory zoning, reflecting different distribution of arsenic, antimony and tellurium and the incorporation of bismuth in some places within the crystal structure (Figure 4, Table 1).

 doi:10.20944/preprints202408.1245.v1

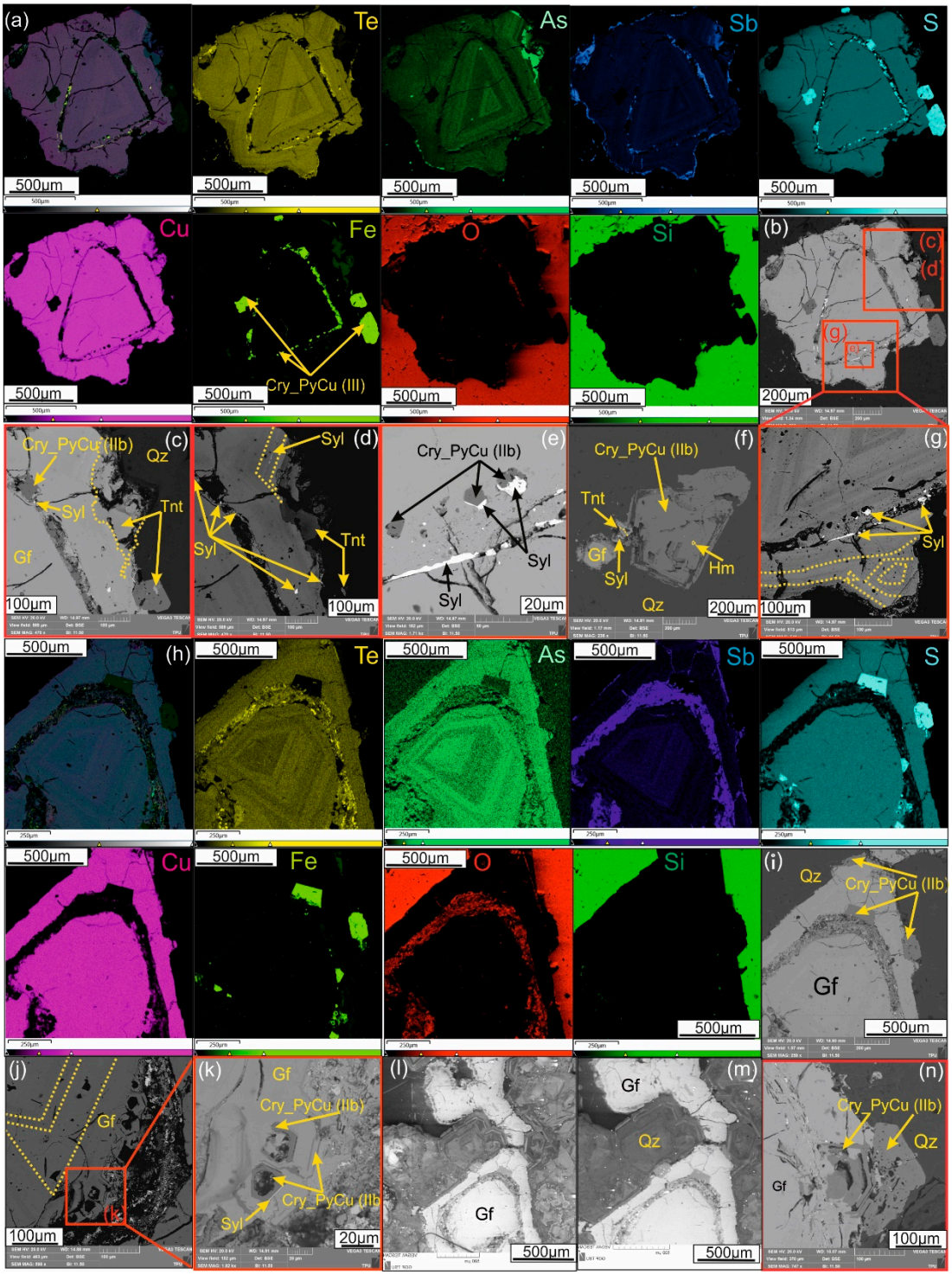

Figure 4. (**a-k, n**) Microphotographs (SEM-BSE-SE images) with X-ray element mapping with distribution of Te, As, Sb, S, Cu, Fe, O, Si, demonstrating goldfieldite (Gf) grains with oscillatory zonation in association with euhedral quartz (Qz) replaced by tennantite (Tnt) (**a-d; f**), and crystalline Cu-bearing pyrite (Cry_PyCu(IIb)) overgrowing with sylvanite (Syl) (**c-e, g-k**) confined to growth zones (i.e. zones of selective replacement of goldfieldite). Hemusite (Hm) is also present as a synchronous growth phase with crystalline Cu-bearing pyrite (Cry_PyCu(IIb)); (**l,m**) cathodoluminescence images demonstrating oscillatory zoned quartz in association with goldfieldite.

Table 1. Representative electron probe microanalyses of TGM, including goldfieldite from the Au-Ag-Te Emmy deposit (Drill hole Em 3).

Depth, m	Cu	Fe	Ag	Zn	Sb	As	Bi	Te	S	Total	Formula:
Tetrahedrite											
31.6	36.05	6.07	1.15	1.86	21.34	6.24	-	-	26.81	99.52	$(Cu_{8.82}Ag_{0.17}Fe_{1.69}Zn_{0.46})(Sb_{2.72}As_{1.29})S_{13}$
38.8	40.58	5.13	-	-	24.89	-	-	3.2	26.00	99.80	$(Cu_{10.24}Fe_{1.47})(Sb_{3.28}Te_{0.4})S_{13}$
49.8	41.97	6.89	-	-	10.49	13.14	-	-	27.35	99.84	$(Cu_{10.06}Fe_{1.88})(As_{2.67}Sb_{1.31})S_{13}$
62.0	40.04	1.46	-	3.94	21.83	2.19	-	4.99	25.55	100.01	$(Cu_{10.28}Zn_{1.01}Fe_{0.43})(Sb_{2.92}Te_{0.64}As_{0.48})S_{13}$
76.2	37.77	6.61	-	-	25.92	3.17	-	-	26.24	99.71	$(Cu_{9.44}Fe_{1.88})(Sb_{3.38}As_{0.67})S_{13}$
83.2	37.27	6.54	-	0.7	27.93	1.73	-	-	25.83	100.00	$(Cu_{9.46}Fe_{1.89}Zn_{0.18})(Sb_{3.7}As_{0.38})S_{13}$
105.6	36.51	4.94	-	2.53	27.06	2.51	-	-	26.45	100.00	$(Cu_{9.05}Fe_{1.39}Zn_{0.63})(Sb_{3.5}As_{0.53})\ S_{13}$
109.8	35.74	9.04	-	-	26.45	2.24	-	-	26.54	100.01	$(Cu_{8.83}Fe_{2.54})(Sb_{3.41}As_{0.47})S_{13}$
Tennantite											
46.4	40.92	7.29	-	-	5.31	16.58	-	-	27.77	100.00	$(Cu_{9.66}Fe_{1.96})(As_{3.32}Sb_{0.65})S_{13}$
46.4	39.37	6.36	-	-	11.68	12.24	-	1.16	26.79	100.00	$(Cu_{9.64}Fe_{1.77})(As_{2.54}Sb_{1.49}Te_{0.14})S_{13}$
46.4	39.57	10.23	-	-	5.52	12.83	-	1.21	28.29	100.00	$(Cu_{9.17}Fe_{2.7})(As_{2.52},Sb_{0.67}Te_{0.14})S_{13}$
46.4	40.08	7.14	-	-	7.93	10,42	-	3.72	27.87	100.00	$(Cu_{9.43}Fe_{1.91})(As_{2.08}Sb_{0.97}Te_{0.44})S_{13}$
49.8	41.01	6.8	-	-	12.42	11,61	-	0.64	27.06	99.54	$(Cu_{9.94}Fe_{1.88})(As_{2.39}Sb_{1.57}Te_{0.08})S_{13}$
55.2	39.6	11.04	-	-	2.67	16,93	-	-	29.75	100.00	$(Cu_{8.73}Fe_{2.77})(As_{3.17}Sb_{0.31})S_{13}$
62.0	40.05	5.11	-	0.98	9.56	15.36	-	2.03	26.74	99.83	$(Cu_{9.82}Fe_{1.43}Zn_{0.24})(As_{3.2}Sb_{1.22}Te_{0.24})S_{13}$
70.2	38.49	8.68	-	-	11.16	13.85	-	-	27.82	100.00	$(Cu_{9.07}Fe_{2.33})(As_{2.77}Sb_{1.37})S_{13}$
76.2	41.99	7.59	-	-	0.84	20.47	-	-	29.11	100.00	$(Cu_{9.46}Fe_{1.95})(As_{3.91}Sb_{0.1})S_{13}$
83.2	42.10	7.62	-	-	1.02	20.31	-	-	28.69	99.74	$(Cu_{9.62}Fe_{1.98})(As_{3.94}Sb_{0.12})S_{13}$
Argentotetrahedrite											
31.6	4.13	5.19	47.38	2	14,55	6,04	-	-	21,17	100,46	$(Ag_{8.65}Cu_{1.28}Fe_{1.83}Zn_{0.62})(Sb_{2.35}As_{1.59})S_{13}$

doi:10.20944/preprints202408.1245.v1

Depth, m	Cu	Fe	Ag	Zn	Sb	As	Bi	Te	S	Total	Formula:
Goldfieldite											
38.2	43.25	0.45	-	-	3.98	3.38	1.50	21.36	26.08	100.00	$(Cu_{10.88}Fe_{0.13})(Te_{2.68}As_{0.72}Sb_{0.52}Bi_{0.11})S_{13}$
38.2	46.19	0.37	-	-	6.87	2.19	-	19.13	25.25	100.00	$(Cu_{12}Fe_{0.11})(Te_{2.47}Sb_{0.93}As_{0.48})S_{13}$
38.2	42.25	1.60	2.39	-	6.11	3.12	-	19.00	25.52	99.99	$(Cu_{10.86}Ag_{0.36}Fe_{0.47})(Te_{2.43}Sb_{0.82}As_{0.68})S_{13}$
38.8	44.93	-	-	-	9.19	2.83	3.01	15.44	24.60	100.00	$Cu_{11.98}(Te_{2.05}Sb_{1.28}As_{0.64}Bi_{0.24})S_{13}$
46.4	43.22	-	-	-	6.42	3.14	-	20.40	27.10	100.29	$Cu_{10.46}(Te_{2.46}Sb_{0.81}As_{0.64})S_{13}$
46.4	43.21	1.84	0.45	-	4.92	2.01	-	19.03	25,81	100.00	$(Cu_{10.98}Ag_{0.07}Fe_{0.53})(Te_{2.41}Sb_{0.65}As_{0.43})S_{13}$
46.4	44.50	1.28	-	-	7.31	1.82	-	17.39	25.65	100.00	$(Cu_{11.38}Fe_{0.37})(Te_{2.21}Sb_{0.98}As_{0.39})S_{13}$
46.4	45.31	-	-	-	9.16	2.66	-	16.45	25.87	99,45	$Cu_{11.49}(Te_{2.08}Sb_{1.21}As_{0.57})S_{13}$
Stibiogoldfieldite											
62.0	43.33	0.38	-	0.81	14.4	1.27	1.99	12.32	25.50	100.00	$(Cu_{11.14}Zn_{0.21}Fe_{0.11})(Sb_{1.93}Te_{1.58}As_{0.28}Bi_{0.16})S_{13}$
Arsenogoldfieldite											
62.0	38.03	6.23	0.72	-	3.94	7.06	2.83	12.83	28.37	100.01	$(Cu_{8.79}Ag_{0.1}Fe_{1.64})(As_{1.38}Te_{1.48}Sb_{0.48}Bi_{0.2})S_{13}$

doi:10.20944/preprints202408.1245.v1

 doi:10.20944/preprints202408.1245.v1

After conducting cathodoluminescence analysis of euhedral quartz, which is associated with goldfieldite, it was found that, similarly to goldfieldite, quartz is characterized by oscillatory zoning (Figure 4l-m) indicating similar conditions for the formation of these crystals.

4.2. APS Minerals

Aluminum-phosphate-sulfate (APS) minerals at the Emmy deposit, occur at a depth of at least ~ 120-150 m below present surface, hosted in both the quartz-dickite and quartz-white mica zones in association with pyrophyllite. Aluminum-phosphate-sulfate minerals occur separately from alunite and barite, which are distributed in relatively near-surface conditions at a depth less than 50 m from the surface (Figure 2b). APS minerals are represented in the deposit by *svanbergite* $SrAl_3(P_{0.5}S_{0.5}O_4)_2(OH)_6$, *woodhouseite* $CaAl_3(P_{0.5}S_{0.5}O_4)_2(OH)_6$ in the central part of APS grains, and *plumbian woodhouseite* $CaAl_3(P_{0.5}S_{0.5}O_4)_2(OH)_6$ in the rims according to their classification of Scott [28], Dill [59], Mills et al. [58].

In the quartz-dickite and quartz-white mica zones, the APS minerals are disseminated in an argillaceous substrate made up of hypogene kaolinite/dickite, pyrophyllite, white mica, and quartz. The varieties, composition and quantities of clay minerals accompanying APS minerals in the bulk rock, are demonstrated in the X-ray diffraction (XRD) pattern of Figure 5. Despite the fact that APS minerals can also be formed during weathering [60], these minerals at Emmy deposit have a hypogene genesis, as they are intimately associated with crystalline pyrite IIb (Figure 6). Their formation is related to the transformation of magmatic apatite, firstly into monazite or xenotime and then to APS, in the deep levels of the advanced argillic alteration zone, in accordance to observations elsewhere (i.e. [61,62]) (Figures 6 and 7).

Mineral		Depth(117.8m)	Depth(133.1m)
Quartz	Qz	59.3	46.08
Pyrite	Py	3.74	23.74
Pyrophyllite	Prl	8.65	19.25
Moganite/Cristobalite	Mog	1.89	2.07
Muscovite/Illite	Ms/Ilt	5.12	3.28
APS	APS	0.2	3.69
Kaolinite	Kln	11.85	1.89
Dickite	Dck	7.14	0.00
Sericite	Ser	2.11	0.00
Summ, %		100.00	100.00

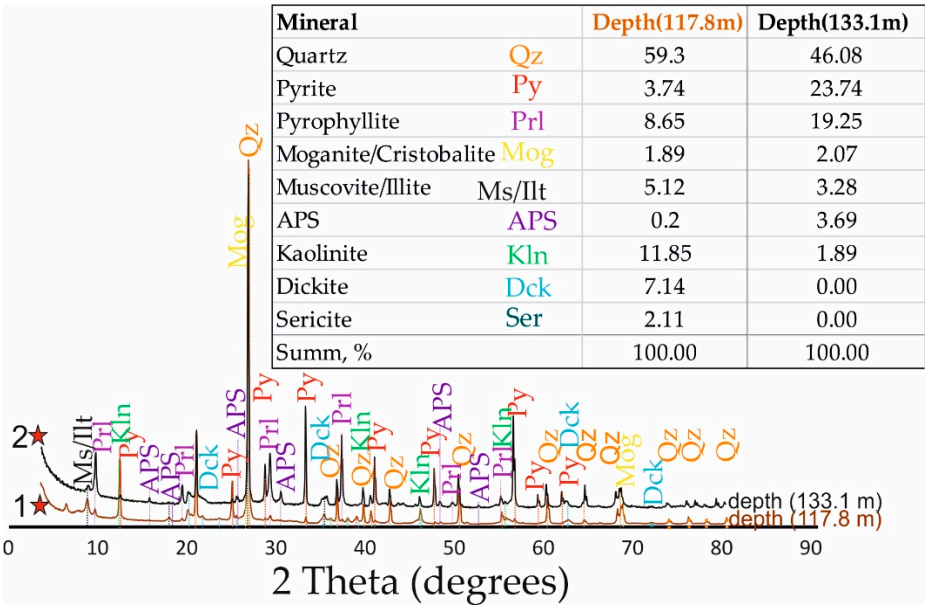

Figure 5. XRD pattern based on bulk composition of APS-bearing rocks. Sampling locations are shown by asterisks on the hydrothermal alteration map and the geological cross section (AB) of Emmy deposit (see Figure 2a and b respectively).

The APS minerals in the Emmy deposit are represented by the beudantite-hinsdalite groups [30,34], and can be classified as calcian svanbergite, svanbergite, strontian woodhouseite, and plumbian woodhouseite (Table 2). They are characterized by a leached and uniform character, predominantly in the intermediate to outer parts (Figure 6). The central part of the APS grains, reflecting the process of apatite dissolution and replacement, is enriched in Sr and Ca (svanbergite and woodhouseite) and rare earth elements (REE), mostly Ce, and is characterized by irregular distribution of these components, causing a fluctuant vermiform randomly distributed pattern (Figure 7a-b). Following the leaching process and the goldfieldite-kawazulite-hemusite mineralization, which is associated with quartz, kaolinite/dickite and pyrite IIb, a new hydrothermal

 doi:10.20944/preprints202408.1245.v1

pulse introduced gold, and enriches the marginal parts of the APS grains with Pb and Ba, forming an oscillatory zoning pattern (Figure 6,7c-d). A similar pattern of grains is confirmed by BSE data, and demonstrates similar features of the internal structure of numerous APS grains (see Figure 6). This pattern of oscillatory zoning is also observed in barite, which is enriched in lead in some zones, where micron-sized grains of gold are observed (Figure 8). In addition to gold this stage was accompanied by fluid enrichment with ore components, especially with TABSS-elements.

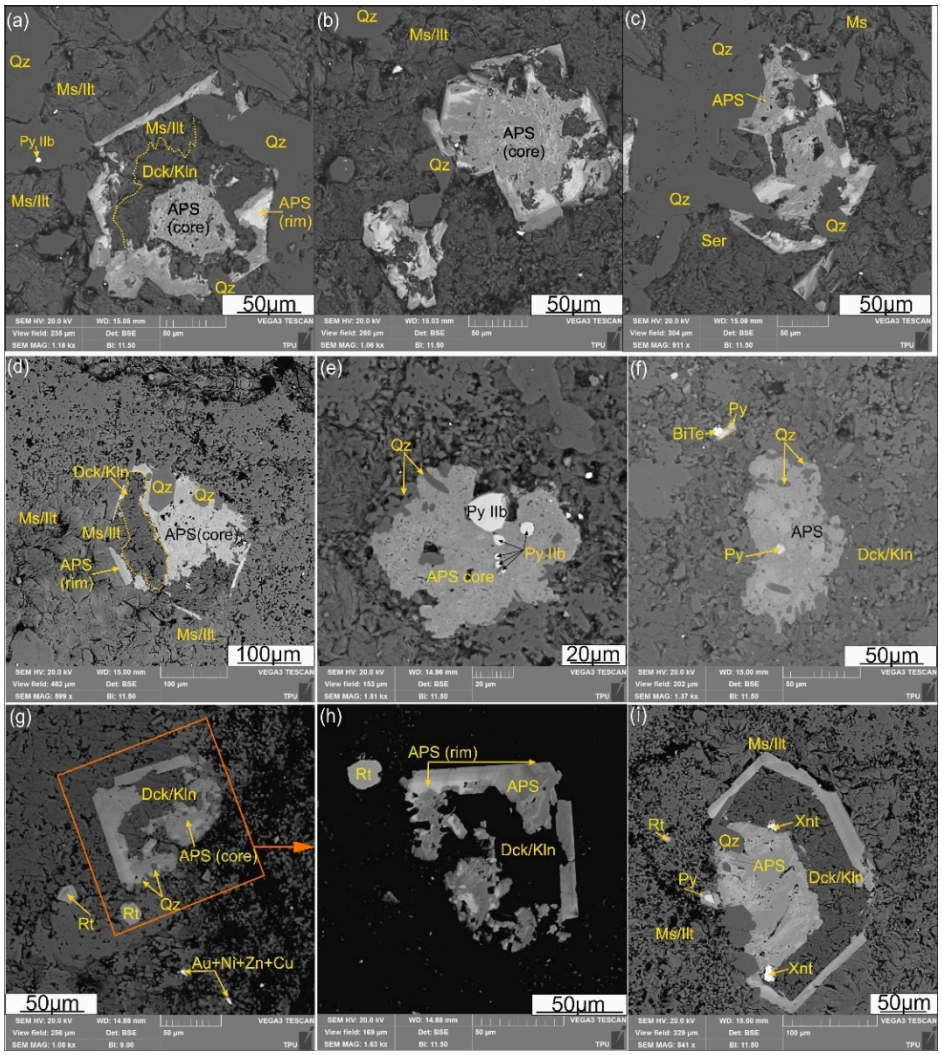

Figure 6. (a-i) Microphotographs (SEM-BSE images) images of aluminum-phosphate-sulfate (APS) minerals from the Emmy deposit (samples collected from the depth of 117.8m, and marked by the first asterisk from figure 2a, XRD bulk sample data see Figure 5). Associated minerals are pyrite (Py IIb), dickite/kaolinite (Dck/Kln), Ms/Ilt (muscovite/illite), xenotime (Xnt), rutile (Rtl) and quartz (Qz), tellurobismuthite (BiTe), and native gold with alloys of Ni,Zn,Cu (Au+Ni+Zn+Cu).

 doi:10.20944/preprints202408.1245.v1

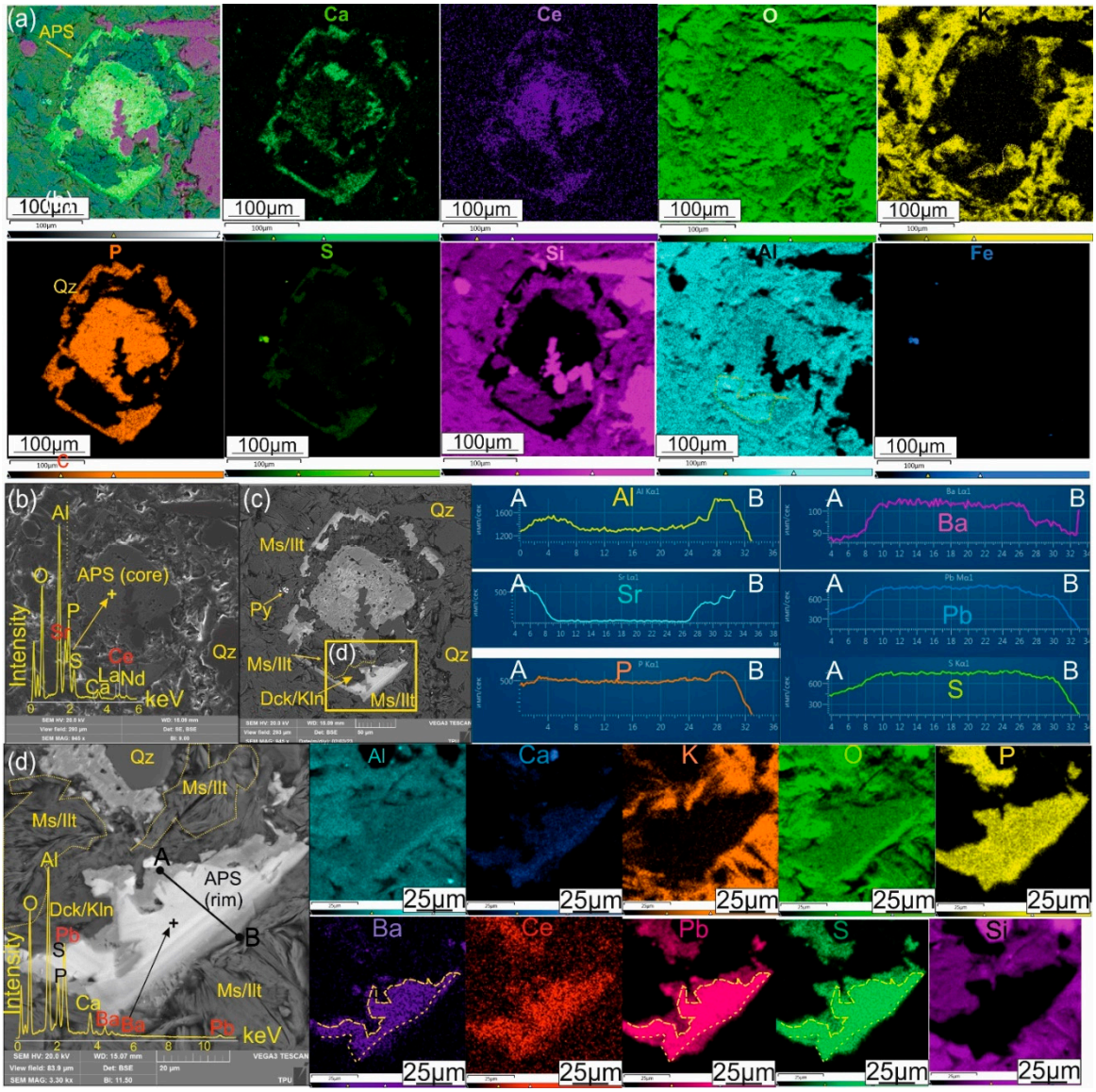

Figure 7. (**a to d**) Microphotographs of aluminum-phosphate-sulfate (APS) mineral in secondary (**b**) and back-scattered (**c-d**) electrons. Multi-element maps illustrate the distribution of Ca, Ce, K, P, S, Al, Si, Fe, Ba, Pb, O within the APS grain and its enlarged fragment; The profile AB, reflects the concentration of trace elements in the absorption edge. Ms/Ilt – muscovite/illite, Dck/Kln – dickite/kaolinite, Py – pyrite, Qz – quartz.

 doi:10.20944/preprints202408.1245.v1

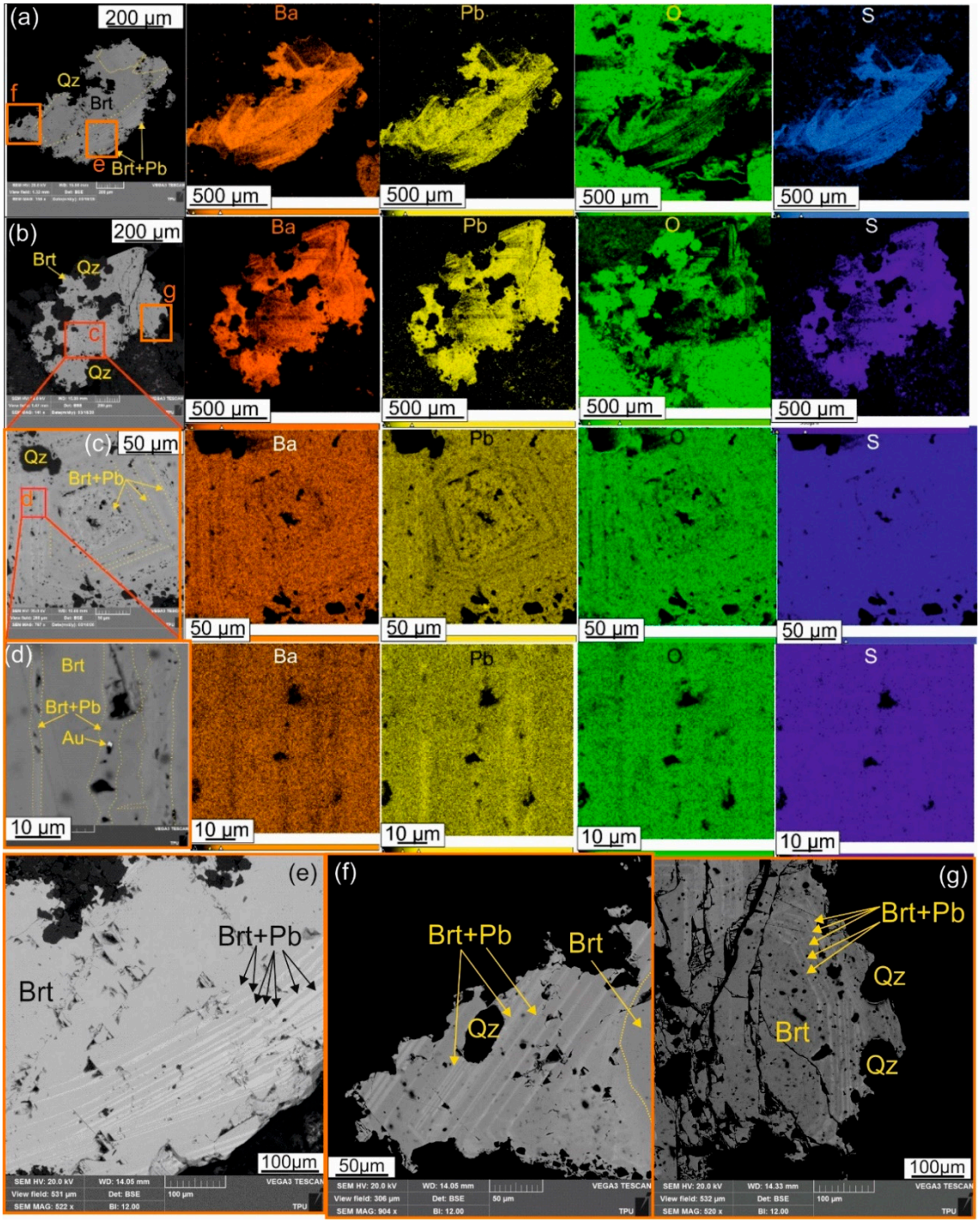

Figure 8. (**a to g**) Microphotographs of barite (Brt) in back-scattered electrons. Multi-element maps illustrate the distribution of Ba, Pb, O, S, within its grains and its enlarged fragments demonstrated oscillatory zonation resulting from enrichment of individual barite zones with lead (Brt+Pb). Qz – quartz, Au – native gold.

Table 2. Representative electron probe microanalyses of APS minerals from the Emmy deposit (bd: below detection).

Nr	Al_2O_3	P_2O_5	SO_3	CaO	SrO	BaO	La_2O_3	Ce_2O_3	Nd_2O_3	PbO	Total	Structural formula based on 11 (O)	Mineral Name
1	32.13	22.19	11.2	3.97	9.38	bd	1.94	3.46	0.85	bd	85.12	$Sr_{0.400}Ca_{0.314}Ce_{0.093}La_{0.053}Nd_{0.022}Al_{2.807}(PO_4)_{1.380}(SO_4)_{0.617}$	Calcian Svanbergite (core)
2	34.02	23.65	10.72	2.23	13.45	bd	2.54	4.33	1.43	bd	92.36	$Sr_{0.556}Ca_{0.170}Ce_{0.113}La_{0.067}Nd_{0.037}Al_{2.867}(PO_4)_{1.425}(SO_4)_{0.571}$	Calcian Svanbergite (core)
3	33.68	22.47	13.32	bd	21.16	bd	bd	bd	bd	bd	90.63	$Sr_{0.848}Al_{2.763}(PO_4)_{1.307}(SO_4)_{0.686}$	Svanbergite (core)
4	33.30	23.75	9.96	2.40	10.89	bd	2.31	4.55	2.36	bd	89.53	$Sr_{0.434}Ca_{0.176}Ce_{0.115}La_{0.059}Nd_{0.058}Al_{2.716}(PO_4)_{1.375}(SO_4)_{0.510}$	Calcian Svanbergite (core)
5	29.69	21.58	9.16	1.25	12.98	bd	1.93	3.11	0.90	bd	80.60	$Sr_{0.616}Ca_{0.109}Ce_{0.093}La_{0.059}Nd_{0.027}Al_{2.873}(PO_4)_{1.493}(SO_4)_{0.562}$	Calcian Svanbergite (core)
6	31.32	20.06	12.19	1.23	18.69	bd	bd	bd	bd	bd	83.49	$Sr_{0.852}Ca_{0.103}Al_{2.905}(PO_4)_{1.333}(SO_4)_{0.717}$	Calcian Svanbergite (core)
7	32.49	22.65	11.10	2.07	13.4	bd	bd	2.29	bd	bd	84.00	$Sr_{0.568}Ca_{0.161}Ce_{0.061}Al_{2.814}(PO_4)_{1.395}(SO_4)_{0.604}$	Calcian Svanbergite (core)
8	28.93	18.34	15.38	1.51	16.43	0.43	bd	bd	bd	bd	81.02	$Sr_{0.784}Ca_{0.134}Ba_{0.013}Al_{2.798}(PO_4)_{1.279}(SO_4)_{0.951}$	Calcian Svanbergite (core)
9	32.05	20.82	13.03	4.96	9.79	bd	1.35	2.69	0.72	bd	85.41	$Sr_{0.426}Ca_{0.399}Ce_{0.074}La_{0.037}Nd_{0.019}Al_{2.840}(PO_4)_{1.319}(SO_4)_{0.731}$	Calcian Svanbergite (core)
10	31.69	22.06	10.38	2.48	11.73	bd	1.86	4.02	1.54	bd	86.64	$Sr_{0.530}Ca_{0.207}Ce_{0.115}La_{0.053}Nd_{0.042}Al_{2.910}(PO_4)_{1.452}(SO_4)_{0.605}$	Calcian Svanbergite (core)
11	31.33	15.53	16.40	3.60	7.00	4.03	bd	bd	bd	11.46	89.54	$Sr_{0.320}Ca_{0.303}Pb_{0.242}Ba_{0.124}Al_{2.910}(PO_4)_{1.034}(SO_4)_{0.968}$	Plumbian Woodhouseite (rim)
12	32.36	22.28	9.76	2.00	12.28	bd	2.06	4.56	1.78	bd	87.08	$Sr_{0.545}Ca_{0.164}Ce_{0.128}La_{0.057}Nd_{0.049}Al_{2.923}(PO_4)_{1.440}(SO_4)_{0.558}$	Calcian Svanbergite (core)
13	33.63	24.96	8.91	1.79	9.77	bd	3.43	6.32	2.35	bd	91.17	$Sr_{0.394}Ce_{0.162}Ca_{0.134}La_{0.088}Nd_{0.058}Al_{2.779}(PO_4)_{1.468}(SO_4)_{0.463}$	Cerian Svanbergite (core)
14	34.47	22.99	11.88	5.54	5.02	0.49	2.41	3.87	1.25	bd	87.92	$Ca_{0.417}Sr_{0.205}Ce_{0.100}La_{0.063}Nd_{0.032}Ba_{0.013}Al_{2.872}(PO_4)_{1.367}(SO_4)_{0.626}$	Strontian Woodhouseite (core)
15	35.70	25.23	10.87	6.44	4.98	bd	3.00	4.79	1.61	bd	92.62	$Ca_{0.462}Sr_{0.193}Ce_{0.117}La_{0.073}Nd_{0.038}Al_{2.825}(PO_4)_{1.424}(SO_4)_{0.544}$	Strontian Woodhouseite (core)
18	29.67	12.49	16.69	4.96	bd	4.54	bd	bd	bd	13.40	81.74	$Ca_{0.412}Pb_{0.280}Ba_{0.137}Al_{2.732}(PO_4)_{0.821}(SO_4)_{0.970}$	Plumbian Woodhouseite (rim)
19	34.67	15.41	19.31	5.73	1.30	5.24	bd	bd	bd	15.49	97.15	$Ca_{0.401}Pb_{0.273}Ba_{0.134}Ce_{0.093}La_{0.053}Sr_{0.049}Nd_{0.022}Al_{2.695}(PO_4)_{0.854}(SO_4)_{0.947}$	Plumbian Woodhouseite (rim)
20	31.67	14.00	18.26	5.16	1.36	5.75	bd	bd	bd	13.93	90.49	$Ca_{0.431}Pb_{0.292}Ba_{0.176}Sr_{0.061}Al_{2.904}(PO_4)_{0.922}(SO_4)_{1.065}$	Plumbian Woodhouseite (rim)
21	31.53	12.13	20.91	5.43	bd	4.31	bd	bd	bd	10.75	86.75	$Ca_{0.439}Pb_{0.218}Ba_{0.127}Al_{2.808}(PO_4)_{0.773}(SO_4)_{1.182}$	Plumbian Woodhouseite (rim)
22	31.35	13.57	18.18	5.44	bd	6.21	bd	bd	bd	11.78	86.54	$Ca_{0.419}Pb_{0.228}Ba_{0.176}Al_{2.684}(PO_4)_{0.829}(SO_4)_{0.982}$	Plumbian Woodhouseite (rim)
23	30.17	12.70	17.70	4.38	bd	5.74	bd	bd	bd	15.68	86.38	$Ca_{0.356}Pb_{0.322}Ba_{0.171}Al_{2.725}(PO_4)_{0.819}(SO_4)_{1.010}$	Plumbian Woodhouseite (rim)

doi:10.20944/preprints202408.1245.v1

 doi:10.20944/preprints202408.1245.v1

4.3. Paragenetic Sequence

To visualize the identification of several stages of mineral formation within the Au-Ag-Te Emmy deposit, the following schematic paragenetic sequence was developed (Table 3). According to this sequence, an early pre-ore alteration stage is followed by a Cu-bearing mineralization, including an early Sn-Mo-Bi-Se-Te-rich (goldfieldite+hemusite+kawazulite) stage, followed by a later As-Sb-Pb-Zn-Au-Ag-Ni-Hg-Bi-Te rich (tetrahedrite-tennantite, galena, chalcopyrite, tellurides, native Au). All these stages are within the stability fields of APS minerals. Goldfieldite can form as part of IS ore assemblages in porphyry-epithermal deposits, however it is also a characteristic mineral in HS mineralogical assemblages too [28,63,64]. Without any presence of typical HS minerals as enargite, luzonite, famatinite, we cannot classify for sure the goldfieldite-hemusite-kawazulite assemblage as of HS type. However, we suggest here a HS affinity for this assemblage, due to its intimate relationship with kaolinite/dickite and pyrophyllite at Emmy deposit. The paragenetic sequence demonstrates an evolution of the system towards lower sulfidation states and more reducing conditions with time.

Table 3. Paragenetic sequence of the Au-Ag-Te Emmy deposit demonstrating mineralogical evolution with time.

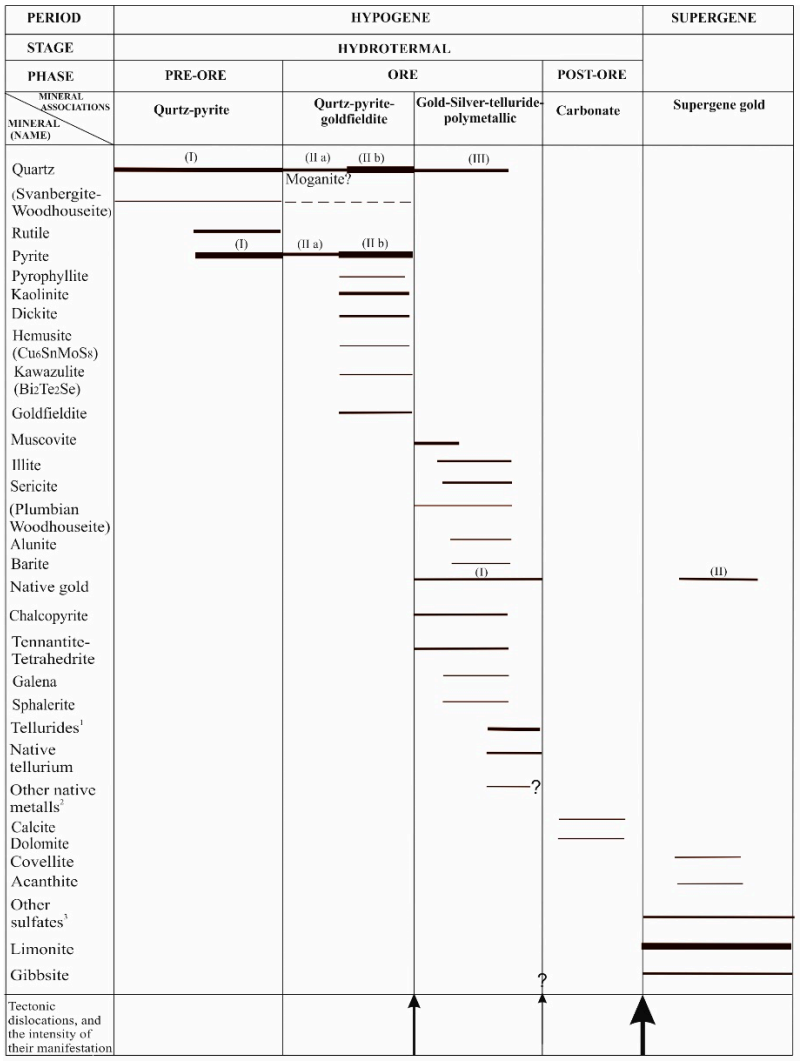

1 Calaverite, krennerite, sylvanite, muthmannite, petzite, hessite, stutzite, coloradoite, melonite, altaite, tellurantimony, tellurobismuthite
2 Native sulfur, tellurium, selenium, bismuth
3 TGM oxidation products, mikasaite, jarosite, anglesite, celestine

 doi:10.20944/preprints202408.1245.v1

5. Discussion

5.1. Sulfides

The formation of two morphological varieties of pyrite II corresponding to the initial mineralization stage and accompanied by golfieldite+hemusite+kawazulite (see Table 3), preceeded the appearance of the telluride stage during the IS-mineralization event, which resulted to a new TABSS-enrichment of the Emmy deposit. The formation of colloform pyrite (IIa) may reflect rapid crystallization during fluid boiling at a hydrothermal fluid–meteoric water interface, creating temperature fluctuations and producing undercooling in the mixed fluid as described by Franchini et al. [65]. As the balance of the mineral-forming system is restored, crystallization of idiomorphic pyrite (IIb) together with minerals enriched in TABSS- elements (goldfieldite, hemusite, kawazulite) and euhedral quartz begins. An open mineral-forming system during this stage, is evidenced by the presence of oscillatory zoning in goldfieldite. The following periodic influx of new mineralized solutions resulted in a renewed mineral-forming system characterized by the transition of goldfieldite to tetrahedrite-tennantite with Te, and the formation of normal tetrahedrite group minerals, tellurides, native tellurium and chalcopyrite.

5.2. Sulfosalts

The formation of oscillatory zoning of sulfosalts (tetrahedrite group minerals) in the epithermal Emmy deposit, is possible attributed to chemical disequilibrium conditions in an open system. Oscillations can be associated with periodic series of pressure release or boiling in geothermal fields [26,27,66,67].

The oscillatory zoning of goldfieldite in the Emmy deposit is represented by both single mineral phase and multiphase zonality and consists in the alternation of bands of different chemical and/or mineral composition (for example, goldfieldite and Bi-bearing goldfieldite).

Single phase zoning, i.e. fluctuations in the Te content are due to changes in the rate of capture of tellurium (and As or Sb) by the growing goldfieldite crystal. The single-phase zoning observed in goldfieldite from Emmy, is characterized by sharp contacts between zone lamellae where it formed as a result of growth banding in an open system and non-equilibrium states (i.e. [27]). The banding is determined by the concentration of these components in the solution layer in direct contact with the growing crystal faces (in the reaction zone). The concentration of an individual component in the reaction zone depends on the ratio of its diffusion rate in solution and the rates of adsorption and desorption of tellurium by the solid phase. This oscillatory zoning could have resulted from rapid changes in the composition of the inflowing fluids or by changes in fluid composition during rapid deposition of the mineral phase, or both. Similar single phase and multiphase oscillatory zoning has been established for goldfieldite from other epithermal high-sulfidation (HS) gold deposits, such as Elshitsa (Bulgaria), Prasolovskoye (Kunashir Island, Kuril Islands) and Ozernovskoye (Kamchatka) [56]. A similar composition of goldfieldite is also characteristic from Pefka and St. Demetrios/Sapes high- and intermediate-sulfidation deposits in northeastern Greece [48].

According to [48,49] inclusions of native Te and tellurides were not formed contemporaneous to goldfieldite, but were rather the result of the new influx of volatiles and metals/metalloids in the system.

This study suggests that, by the time the new fluid impulse was introduced at Emmy deposit, the arseno- and stibiogoldfieldite crystals had not yet completely crystallized, as evidenced by plastic deformations and continued grain growth. The new influx was also enriched in addition to metals (Au, Ag, Hg, and other elements).

5.3. Sulfates

The APS minerals occur mainly within zones of advanced argillic and transitional advanced argillic to sericitic alteration zones in several porphyry and high-sulfidation epithermal deposits at, for example, Lepanto [3], Baquio [68], El Salvador [69], Summitville, La Granja, La Escondida [62],

 doi:10.20944/preprints202408.1245.v1

and Melitena and Sapes [21,64]. Analysis of APS mineral compositions can reveal useful information regarding local conditions of formation with respect to fluid composition, pH, and fO_2 [62].

The central parts of aluminum-phosphate-sulfate (APS) minerals present in the Emmy deposit are Ca-Sr-Ce-dominant APS minerals that fall within the svanbergite-woodhouseite compositional field. This parts of APS minerals at Emmy deposit were deposited during an initial stage of primary apatite and alkali earth elements dissolution by acid solutions of magmatic-hydrothermal origin, as suggested by Stoffregen and Alpers [62]. Subsequent hydrothermal alteration in the Emmy deposit, leaches these grains due to the incursion of reactive acidic solution in the system, resulting in crystallization of plumbian woodhouseite in the rims of the APS grains.

In a detailed analysis of elemental maps and as a result of the distribution of elements within the studied grains of APS, it was found that sulfur, together with lead and barium enriches the marginal zone, characterized by oscillatory zoning, while the central part of the grains is enriched with cerium, strontium and calcium. Between these two parts of the crystals there is a break or a sharp change in crystallization conditions, possibly due to the process of boiling or mixing of the fluid, accompanied by precipitation of the mineralization, which is associated with pyrite IIb, goldfieldite, kawazulite and hemusite. This crystallization of Pb-bearing APS minerals (i.e. hinsdalite) with pyrite occur in the Summitville gold-copper deposit (Colorado) [62] and the Mavrokoryfi HS silver-gold-copper prospect (Greece) [64]. The marginal parts of APS minerals at Emmy deposit exhibit preferential sorption of Pb. This enrichment may indicate proximity to a porphyry-style mineralization at depth as stated for Melitena porphyry-epithermal prospect (Greece) by Voudouris and Melfos [62].

In view of the fact that we observe a repeating pattern of oscillating texture in different grains of APS minerals in the studied material, we conclude that these textures are the result of external conditions, i.e. the behavior of the general ore-forming hydrothermal process, and are not related with the internal self-organization of individual APS grains. In the latter case the grains should have of a more individual internal structure without a regular alternation of zones.

In the upper parts of the advanced argillic alteration zone, barite, similarly to APS minerals demonstrates oscillatory zonation within the grains and exhibit preferential sorption of Pb, confirming a change in external conditions of mineralization process of Emmy deposit.

6. Conclusions

Based on mineralogical and petrographic studies, and in particular of sulfides (pyrite), sulfosalts (goldfieldite) and sulfates (APS minerals and barite), it was established that within the Au-Ag-Te Emmy deposit, periods of rapid deposition of ore, due to boiling of solutions at a hydrothermal fluid–meteoric water interface, were followed by long-lasting conditions of mineral formation in an open ore-forming system.

Copper-bearing pyrite of a collomorphic texture may indicate a rapid process of precipitation during abrupt cooling from boiling solutions together with moganite. The subsequent formation of euhedral crystals of Cu-bearing pyrite, bordering the collomorphic pyrite, is attributed to a slow crystallization in a quiescent formation environment. Under these conditions the system was open, as evidenced by the oscillatory zoned goldfieldite, accompanying crystalline Cu-bearing pyrite, emphasizing the rhythmic change of growth zones of enrichment in either arsenic or tellurium.

A similar textural pattern, confirming the presence of a non-equilibrium state of the Emmy deposit, was found by studying euhedral quartz, and APS minerals in their marginal parts of the grains, by using cathodoluminescence.

We consider goldfieldite to be part of a HS mineral association at Emmy, followed by an IS assemblage composed of tennantite-tetrahedrite group, tellurides and native tellurium correspond to new influx of Te, Sb and As. Goldfieldite was replaced by native tellurium and tellurides along its growth zones. The observed replacement of goldfieldite by the tellurides of mercury, nickel, lead and copper is attributed to a new influx of volatiles and metals/metalloids into the open mineral-forming system.

 doi:10.20944/preprints202408.1245.v1

The APS minerals at the deep levels of the advanced argillic alteration of Emmy deposit, are represented by members of the svanbergite-woodhouseite series. Element mapping of the APS minerals, indicated lead enrichment in the marginal, oscillatory zoned part of the grains, while the intermediate parts of the APS grains are leached. These two parts of the grains are probably related to the two phases of the mineralization, i.e. late influx of IS fluids vs deposition of goldfieldite-kawazulite-hemusite assemblage respectivly. The central part of the APS grains is enriched in cerium and strontium, and was formed during the pre-ore stage, as a result of apatite replacement. Barite found in the upper level of the advanced argillic alteration zone, is characterized by oscillatory zoning and by lead-enrichment of individual zones too.

This study demonstrates the fundamental importance of external processes as reflected by the evolution of the physicochemical conditions of mineral formation, both from a fundamental genetic and applied exploratory point of view. This determines the fundamental importance of these processes and can be used when planning geological exploration work on analogous deposits in the territory of the Khabarovsk Territory and beyond.

Author Contributions: Conceptualization, supervision, project administration, investigation, writing—original draft preparation T.Yu. Yakich; Writing—review and editing P. Voundouris; Methodology, resources, development of a map of alteration zoning and data curation D.V. Levochskaia; Carrying out bulk XRD analysis M.V. Shaldybin and its interpreting result Y. M. Lopushnyak; Funding acquisition M.A. Rudmin and A. S. Ruban; Data curation A. E. Erofeev and A. K. Mazurov, Sample preparation P. N. Maximov, M.S. Minakov, Analytical data K.V. Bestemianova and E.A. Sinkina. All authors have read and agreed to the published version of the manuscript.

Funding: The research was supported by Ministry of Science and Higher Education of the Russian Federation (project FSWW-2023-0010).

Acknowledgments: The authors thank the editor and anonymous reviewers for their constructive reviews, which led to the improvement of the manuscript.

Conflicts of Interest: The authors declare no conflict of interest.

References

1. Hedenquist, J.W.; Izawa, E.; Arribas Jr, A.; White, N.C. Epithermal Gold Deposits: Styles, Characteristics, and Exploration: Resource Geology Special Publication. *SEG Newsl.* **1995**, 9–13.
2. Hedenquist, J.W.; Izawa, E.; Arribas, A.; White, N.C. Epithermal Gold Deposits: Styles, Characteristics and Exploration. *Resour. Geol.* **1996**, *1*, 9–13.
3. Hedenquist, J.W.; Arribas, A.; Reynolds, T.J. Evolution of an Intrusion-Centered Hydrothermal System: Far Southeast-Lepanto Porphyry and Epithermal Cu-Au Deposits, Philippines. *Econ. Geol.* **1998**, *93*, 373–404, doi:10.2113/gsecongeo.93.4.373.
4. Sillitoe, R.H.; Thompson, J.F.H. Intrusion-Related Vein Gold Deposits: Types, Tectono-Magmatic Settings and Difficulties of Distinction from Orogenic Gold Deposits. *Resour. Geol.* **1998**, *48*, 237–250, doi:10.1111/j.1751-3928.1998.tb00021.x.
5. Yakich, T.Y.; Nikolaeva, A.N.; Bukhanova, D.S.; Maximov, P.N.; Sinkina, E.A.; Kutyrev, A. V.; Sarsekeeva, E.M.; Zhegunov, P.S.; Levochskaya, D. V.; Rudmin, M.A. Mineral Features of the Copper Association of the Baranevskoe Epithermal Deposit (Central Kamchatka). *Bull. Tomsk Polytech. Univ. Geo Assets Eng.* **2022**, *333*, 74–87, doi:10.18799/24131830/2022/12/3860.
6. Levochskaya, D. V.; Yakich, T.Y.; Lesniak, D.V.; Ananyev, Y.S. Hydrothermal-Altered Zoning, Fluid Conditions, and Types of Gold Mineralization within the Elena and Emy Deposits of the Epithermal Svetloye Ore District (Khabarovsk Territory). *Bull. Tomsk Polytech. Univ. Geo Assets Eng.* **2021**, *332*, 17–32, doi:10.18799/24131830/2021/10/3252.
7. Hattori, K.H.; Arai, S.; Clarke Barrie, D.B. Selenium, Tellurium, Arsenic and Antimony Contents of Primary Mantle Sulfides. *Can. Mineral.* **2002**, *40*, 637–650, doi:10.2113/gscanmin.40.2.637.
8. Helmy, H.M.; Ballhaus, C.; Berndt, J.; Bockrath, C.; Wohlgemuth-Ueberwasser, C. Formation of Pt, Pd and Ni Tellurides: Experiments in Sulfide-Telluride Systems. *Contrib. to Mineral. Petrol.* **2007**, *153*, 577–591, doi:10.1007/s00410-006-0163-7.

9. König, S.; Eickmann, B.; Zack, T.; Yierpan, A.; Wille, M.; Taubald, H.; Schoenberg, R. Redox Induced Sulfur-Selenium Isotope Decoupling Recorded in Pyrite. *Geochim. Cosmochim. Acta* **2019**, *244*, 24–39, doi:10.1016/j.gca.2018.09.013.
10. Marfin, A.E.; Ivanov, A. V.; Abramova, V.D.; Anziferova, T.N.; Radomskaya, T.A.; Yakich, T.Y.; Bestemianova, K. V. A Trace Element Classification Tree for Chalcopyrite from Oktyabrsk Deposit, Norilsk–Talnakh Ore District, Russia: La-Icpms Study. *Minerals* **2020**, *10*, 1–15, doi:10.3390/min10080716.
11. Börner, F. In-Situ Trace Element and S Isotope Systematics in Porphyry-Epithermal Pyrite , Limnos Island , Greece.; 2021.
12. Cook, N.J.; Ciobanu, C.L.; Spry, P.G.; Voudouris, P. Understanding Gold-(Silver)-Telluride-(Selenide) Mineral Deposits. *Episodes* **2009**, *32*, 249–263.
13. Cook, N.J.; Ciobanu, C.L. Mineral Deposit Research: Meeting the Global Challenge. *Miner. Depos. Res. Meet. Glob. Chall.* **2005**, doi:10.1007/3-540-27946-6.
14. Spry, P.G.; Foster, F.; Truckle, J.S.; Chadwick, T.H. The Mineralogy of the Golden Sunlight Gold-Silver Telluride Deposit, Whitehall, Montana, U.S.A. *Mineral. Petrol.* **1997**, *59*, 143–164, doi:10.1007/bf01161857.
15. Pals, D.W.; Spry, P.G.; Chryssoulis, S. Invisible Gold and Tellurium in Arsenic-Rich Pyrite from the Emperor Gold Deposit, Fiji: Implications for Gold Distribution and Deposition. *Econ. Geol.* **2003**, *98*, 479–493.
16. Cook, N.J.; Ciobanu, C.L.; Mao, J. Textural Control on Gold Distribution in As-Free Pyrite from the Dongping, Huangtuliang and Hougou Gold Deposits, North China Craton (Hebei Province, China). *Chem. Geol.* **2009**, *264*, 101–121, doi:10.1016/j.chemgeo.2009.02.020.
17. Cooke, D.R.; McPhail, A.D.C. Epithermal Au-Ag- Te Mineralization, Acupan, Baguio District, Philippines: Numerical Simulations of Mineral Deposition. *Econ. Geol.* **2001**, *96*, 109–131.
18. Cook, N.J.; Ciobanu, C.L. Bismuth Tellurides and Sulphosalts from the Larga Hydrothermal System, Metaliferi Mts , Romania: Paragenesis and Genetic Significance. *Mineral. Mag.* **2004**, *68*, 301–321, doi:10.1180/0026461046820188.
19. Kovalenker, V.A.; Safonov, Y.G.; Naumov, V.B.; Rusinov, V.L. The Epithermal Gold-Telluride Kochbulak Deposit (Uzbekistan). *Geol. Ore Depos.* **1997**, *39*, 107–128.
20. Plotinskaya, O.Y.; Kovalenker, V.A.; Seltmann, R.; Stanley, C.J. Te and Se Mineralogy of the High-Sulfidation Kochbulak and Kairagach Epithermal Gold Telluride Deposits (Kurama Ridge, Middle Tien Shan, Uzbekistan). *Mineral. Petrol.* **2006**, *87*, 187–207, doi:10.1007/s00710-006-0130-z.
21. Voudouris, Panagiotis; Melfos, V. Aluminum-Phosphate-Sulfate (APS) Minerals in the Sericitic-Advanced Argillic Alteration Zone of the Melitena Porphyry-Epithermal Mo-Cu ± Au ± Re Prospect, Western Thrace, Greece. *Neues Jahrb. für Mineral.* **2013**, *190*, 11–27.
22. Sidorov, E.G.; Borovikov, A.A.; Tolstykh, N.D.; Bukhanova, D.S.; Palyanova, G.A.; Chubarov, V.M. Au (Ag)-Se-Te-s-Cu-Sb-as-Bi Mineralization at the Maletoyvayam Deposit (Central Kamchatka, Russia) and Physicochemical Conditions of Its Formation. *Minerals* **2020**, *10*, 1–19, doi:10.3390/min10121093.
23. Tolstykh, N.D.; Palyanova, G.A.; Bobrova, O. V.; Sidorov, E.G. Mustard Gold of the Gaching Ore Deposit (Maletoyvayam Ore Field, Kamchatka, Russia). *Minerals* **2019**, *9*, 1–18, doi:10.3390/min9080489.
24. Yakich, T.Y.; Ananyev, Y.S.; Ruban, A.S.; Gavrilov, R.Y.; Lesnyak, D.V.; Levochskaia, D.V.; Savinova, O.V.; M.A., R. Mineralogy of the Svetloye Epithermal District, Okhotsk-Chukotka Volcanic Belt, and Its Insights for Exploration. *Ore Geol. Rev.* **2021**, *136*, doi:10.1016/j.oregeorev.2021.104257.
25. Ortoleva, P., Merino, E., Moore, C., & Chadam, J. Geochemical Self-Organization I; Reaction-Transport Feedbacks and Modeling Approach. *Am. J. Sci.* **1987**, *287*, 979–1007.
26. Shore, M.; Fowler, A.D. Oscillatory Zoning in Minerals: A Common Phenomenon. *Can. Mineral.* **1996**, *34*, 1111–1126.
27. Holten, T.; Jamtveit, B.; Meakin, P. Noise and Oscillatory Zoning of Minerals. *Geochim. Cosmochim. Acta* **2000**, *64*, 1893–1904, doi:10.1016/S0016-7037(99)00444-5.
28. Plotinskaya, O.Y.; Rusinov, V.L.; Kovalenker, V.A.; SELTMANN, R. Oscillatory Zoning in Goldfieldite as a Possible Indicator of It's Formation Conditions. *Bulg. Acad. Sci. Geochemistry, Mineral. Petrol.* **2005**, *43*, 142–147.
29. George, L.; Cook, J.; Stanley, J.; Welch, D. Revision 1 The Tetrahedrite Group : Nomenclature and Classification. **2020**, 2–43.
30. Scott, K.M. Solid Solution in, and Classification of, Gossan-Derived Members of the Alunite-Jarosite Family, Northwest Queensland, Australia. *Am. Mineral.* **1987**, *72*, 178–187.

31. Jambor, J.L. Nomenclature of the Alunite Supergroup. *Can. Mineral.* **1999**, *37*, 1323–1341.
32. Jambor, J.L. Nomenclature of the Alunite Supergroup:Reply. *Can. Mineral.* **2000**, *38*, 1298–1303.
33. Keith M. Scott Nomenclature of the Alunite Supergroup:Discussion. *Can. Mineral.* **2000**, *38*, 1295–1297.
34. Mills, S.J.; Hatert, F.; Nickel, E.H.; Ferraris, G. The Standardisation of Mineral Group Hierarchies: Application to Recent Nomenclature Proposals. *Eur. J. Mineral.* **2009**, *21*, 1073–1080, doi:10.1127/0935-1221/2009/0021-1994.
35. Tikhomirov, P.L.; Akinin, V. V.; Ispolatov, V.O.; Alexander, P.; Cherepanova, I.Y.; Zagoskin, V. V. The Okhotsk-Chukotka Volcanic Belt: Age of Its Northern Part According to New Ar-Ar and U-Pb Geochronological Data. *Stratigr. Geol. Correl.* **2006**, *14*, 524–537, doi:10.1134/S0869593806050054.
36. Ananyev, Y.S.; Zhitkov, V.G.; Potseluev, A.A. Forecasting and Prospecting Model of Epithermal High Sulfidation Au7AG Deposits Using Modern Satellite Data (on the Example of Ore Field Svetloe, Khabarovskiy Kray). *Bull. Tomsk Polytech. Univ. Geo Assets Eng.* **2019**, *330*, 84–92.
37. Lesnyak, D. V.; Ananyev, Y.S.; Gavrilov, R.Y. Structural, Geophysical and Geochemical Criteria for Epithermal High-Sulfidation Gold Mineralization on the Example of Svetloe Ore Field (Khabarovskiy Kray). *Bull. Tomsk Polytech. Univ. Geo Assets Eng.* **2022**, *333*, 60–72.
38. Moore, D.M.; Reynolds, Jr., R.C. *Diffraction and the Identification and Analysis of Clay Minerals*; Oxford University Press: Oxford, 1997;
39. Bish, D.L.; Post, J.E. Quantitative Mineralogical Analysis Using the Rietveld Fullpattern Fitting Method. *Am. Mineral.* **1993**, *78*, 932–940.
40. Taylor, J.C. Computer Programs for Standardless Quantitative Analysis of Minerals Using the Full Powder Diffraction Profile. *Powder Diffr.* **1991**, *6*, 2–9.
41. Cherkasova, T.; Kucherenko, I.; Abramova, R. Rear Polymineral Zone of Near-Veined Metasomatic Aureole in Mesothermal Zun-Holba Gold Deposit (Eastern Sayan). In Proceedings of the IOP Conference Series: Earth and Environmental Science; 2015; Vol. 27.
42. Keith, M.; Smith, D.J.; Jenkin, G.R.T.; Holwell, D.A.; Dye, M.D. A Review of Te and Se Systematics in Hydrothermal Pyrite from Precious Metal Deposits: Insights into Ore-Forming Processes. *Ore Geol. Rev.* **2018**, *96*, 269–282, doi:10.1016/j.oregeorev.2017.07.023.
43. Timkin, T.; Voroshilov, V.; Askanakova, O.; Cherkasova, T.; Chernyshov, A.; Korotchenko, T. Estimating Gold-Ore Mineralization Potential within Topolninsk Ore Field (Gorny Altai). In Proceedings of the IOP Conference Series: Earth and Environmental Science; 2015; Vol. 27.
44. Keith, M.; Smith, D.J.; Jenkin, G.R.J.; Holwell, D.A. Global Se and Te Systematics in Hydrothermal Pyrite from Different Ore Deposits: A Review. *Appl. Earth Sci.* **2017**, *126*, 70–71, doi:10.1080/03717453.2017.1306265.
45. Keith, M.; Börner, F.; Smith, D.J.; Barry, T.L.; Neumann, T.; Klemd, R. Epithermal Pyrite as Target for Tellurium Exploration in Vatukoula , Fiji. *Abstr. DMG virtual poster Sess.* **2020**, 2–3.
46. Biagioni C., George L.L., Cook N.J., Makovicky E., Moëlo Y., Pasero M., Sejkora J., Stanley C.J., W.M.D. and B.F. The Tetrahedrite Group: Nomenclature and Classification. *Am. Mineral.* **2020**, *105*, 109–122.
47. Plotinskaya, O.Y.; Grabezhev, A.I.; Seltmann, R. Fahlores Compositional Zoning in Porphyry-Epithermal System: The Biksizak Occurrence, South Urals, Russia as Example. *Geol. Ore Depos.* **2015**, *57*, 48-70 (in Russia).
48. Repstock, A.; Voudouris, P.; Zeug, M.; Melfos, V.; Zhai, M.; Li, H.; Kartal, T.; Matuszczak, J. Chemical Composition and Varieties of Fahlore-Group Minerals from Oligocene Mineralization in the Rhodope Area, Southern Bulgaria and Northern Greece. *Mineral. Petrol.* **2016**, *110*, 103–123, doi:10.1007/s00710-015-0412-4.
49. Repstock, A.; Voudouris, P.; Kolitsch, U. New Occurrences of Watanabeite, Colusite, "Arsenosulvanite" and "Cu-Excess" Tetrahedrite-Tennantite at the Pef Ka High-Sulfidation Epithermal Deposit, Northeastern Greece. *Neues Jahrb. fur Mineral. Abhandlungen* **2015**, *192*, 135–149, doi:10.1127/njma/2015/0276.
50. Staude, S.; Mordhorst, T.; Neumann, R.; Prebeck, W.; Markl, G. Compositional Variation of the Tennantite–Tetrahedrite Solid-Solution Series in the Schwarzwald Ore District (SW Germany): The Role of Mineralization Processes and Fluid Source. *Mineral. Mag.* **2010**, *74*, 309–339, doi:10.1180/minmag.2010.074.2.309.
51. Arlt, T.; Diamond, L.W. Composition of Tetrahedrite-Tennantite and 'Schwazite' in the Schwaz Silver Mines, North Tyrol, Austria. *Mineral. Mag.* **1998**, *62*, 801–820, doi:10.1180/002646198548188.

52. Krismer, M.; Vavtar, F.; Tropper, P.; Kaindl, R.; Sartory, B. The Chemical Composition of Tetrahedrite-Tennantite Ores from the Prehistoric and Historic Schwaz and Brixlegg Mining Areas (North Tyrol, Austria). *Eur. J. Mineral.* **2011**, *23*, 925–936, doi:10.1127/0935-1221/2011/0023-2137.
53. Lyubimtseva, N.G.; Bortnikov, N.S.; Borisovsky, S.E. Coexisting Bournonite–Seligmannite and Tennantite–Tetrahedrite Solid Solutions of the Darasun Gold Deposit, Eastern Transbaikalia, Russia: Estimation of the Mineral Formation Temperature. *Geol. Ore Depos.* **2019**, *61*, 274–291, doi:10.1134/S1075701519030061.
54. Keim, M.F.; Walter, B.F.; Neumann, U.; Kreissl, S.; Bayerl, R.; Markl, G. Polyphase Enrichment and Redistribution Processes in Silver-Rich Mineral Associations of the Hydrothermal Fluorite-Barite-(Ag-Cu) Clara Deposit, SW Germany. *Miner. Depos.* **2019**, *54*, 155–174, doi:10.1007/s00126-018-0799-z.
55. Hu, Y.; Ye, L.; Li, Z.; Huang, Z.; Zhang, J. Genesis of Fahlore in the Tianbaoshan Lead–Zinc Deposit, Sichuan Province, China: A Scanning Electron Microscopy–Energy Dispersive Spectroscopy Study. *Acta Geochim.* **2018**, *37*, 842–853, doi:10.1007/s11631-018-0280-9.
56. Plotinskaya, O.; Grabezhev, A.; Seltmann, R. Fahlores Compositional Zoning in a Porphyry-Epithermal System: Biksizak Occurrence, South Urals, Russia as an Example. *Geol. Ore Depos.* **2015**, *57*, 48–70, doi:10.7868/s0016777015010037.
57. Biagioni, C.; Sejkora, J.; Musetti, S.; Makovicky, E.; Pagano, R.; Pasero, M.; Dolníček, Z. Stibiogoldfieldite, Cu 12 (Sb 2 Te 2)S 13 , a New Tetrahedrite-Group Mineral . *Mineral. Mag.* **2022**, *86*, 168–175, doi:10.1180/mgm.2021.107.
58. Sejkora, J.; Biagioni, C.; Dolníˇcek, Z.; Voudouris, P. Arsenogoldfieldite, IMA 2022- 084. *CNMNC Newsl. 70, Eur. J. Miner.* **2022**, *34*.
59. Dill, H.G. The Geology of Aluminum Phosphate and Sulphates of the Alunite Group Minerals: A Review. *Earth Sci. Rev.* **2001**, *53*, 35–93, doi:10.1016/S0012-8252(00)00035-0.
60. Yanchenko, O.M.; Timkin, T.V.; Voroshilov, V.G.; Yakich, T.Y.; Mansour, Z. Nature of Phosphate Distribution within the Golden Weathering Crusts of the Tomsk Region. *Bull. Tomsk Polytech. Univ. Geo Assets Eng.* **2021**, *332*, 74–91, doi:10.18799/24131830/2021/9/3355.
61. Brimhall, G.H.; Ghiorso, M.S. Origin and Ore-Forming Consequences of the Advanced Argillic Alteration Process in Hydrogene Environments by Magmatic Gas Contamination of Meteoric Fluids. *Econ. Geol.* **1983**, *78*, 73–90, doi:10.2113/gsecongeo.78.1.73.
62. Stoffregen, R.E.; Alpers, C.N.; States, U.; Survey, G.; Bypass, Y. Woodhouseite and Svanbergite in Hydrothermal Ore Deposits: Products of Apatite Destruction during Advanced Argillic Alteration. *Can. Mineral.* **1987**, *25*, 201–211.
63. Trudu, A.G.; Knittel, U. Crystallography, Mineral Chemistry and Chemical Nomenclature of Goldfieldite, the Tellurian Member of the Tetrahedrite Solid-Solution Series. *Can. Mineral.* **1998**, *36*, 1115–1137.
64. Voudouris, P.C. Conditions of Formation of the Mavrokoryfi High-Sulfidation Epithermal Cu-Ag-Au-Te Mineralization (Petrota Graben, NE Greece). *Mineral. Petrol.* **2011**, *101*, 97–113, doi:10.1007/s00710-010-0139-1.
65. Franchini, M.; McFarlane, C.; Maydagán, L.; Reich, M.; Lentz, D.R.; Meinert, L.; Bouhier, V. Trace Metals in Pyrite and Marcasite from the Agua Rica Porphyry-High Sulfidation Epithermal Deposit, Catamarca, Argentina: Textural Features and Metal Zoning at the Porphyry to Epithermal Transition. *Ore Geol. Rev.* **2015**, *66*, 366–387, doi:10.1016/j.oregeorev.2014.10.022.
66. Tardani, D.; Reich, M.; Deditius, A.P.; Chryssoulis, S.; Sánchez-Alfaro, P.; Wrage, J.; Roberts, M.P. Copper–Arsenic Decoupling in an Active Geothermal System: A Link between Pyrite and Fluid Composition. *Geochim. Cosmochim. Acta* **2017**, *204*, 179–204, doi:10.1016/j.gca.2017.01.044.
67. García-Ruiz, J.M.; Otálora, F. *Crystal Growth in Geology: Patterns on the Rocks*; 2015; Vol. 2; ISBN 9780444633064.
68. Aoki, M.; Comsti, E.; Lazo, F.; Matsuhisa, Y. Advanced Argillic Alteration and Geochemistry of Alunite in an Evolving Hydrothermal System at Baguio, Northern Luzon, Phillipines. *Resour. Geol.* **1993**, *43*, 155–164.
69. Watanabe, Y.; Hedenquist, J. Mineralogical and Stable Isotope Zonation at the Surface over the El Salvador Porphyry Cu Deposit, Chile. *Econ. Geol.* **2001**, *96*, 1775–1797, doi:10.2113/96.8.1775.
70. Voudouris, P.C.; Melfos, V.; Spry, P.G.; Moritz, R.; Papavassiliou, C.; Falalakis, G. Mineralogy and Geochemical Environment of Formation of the Perama Hill High-Sulfidation Epithermal Au-Ag-Te-Se Deposit, Petrota Graben, NE Greece. *Mineral. Petrol.* **2011**, *103*, 79–100, doi:10.1007/s00710-011-0160-z.
71. Voudouris, P.C.; Melfos, V.; Spry, P.G.; Kartal, T.; Schleicher, H.; Moritz, R.; Ortelli, M. The Pagoni Rachi/Kirki Cu-Mo±Re±Au Deposit, Northern Greece: Mineralogical and Fluid Inclusion Constraints on

 doi:10.20944/preprints202408.1245.v1

the Evolution of a Telescoped Porphyry-Epithermal System. *Can. Mineral.* **2013**, *51*, 253–284, doi:10.3749/canmin.51.2.253.